Optimizing tuberculosis treatment efficacy: comparing the standard regimen with Moxifloxacin-containing regimens

Maral Budak[1], Joseph M. Cicchese[2], Pauline Maiello[3], H. Jacob Borish[3], Alexander G. White[3], Harris B. Chishti[3], Jaime Tomko[3], L. James Frye[3], Daniel Fillmore[3], Kara Kracinovsky[3], Jennifer Sakal[3], Charles A. Scanga[3], Philana Ling Lin[3], Véronique Dartois[4,5], Jennifer J. Linderman[2], JoAnne L. Flynn[3], Denise E. Kirschner[1]*

[1] Department of Microbiology and Immunology, University of Michigan Medical School, 1150 W Medical Center Drive, 5641 Medical Science II, Ann Arbor, MI 48109-5620

[2] Department of Chemical Engineering, University of Michigan, G045W NCRC B28, 2800 Plymouth Rd, Ann Arbor, MI 48109-2136

[3] Department of Microbiology and Molecular Genetics and Center for Vaccine Research, University of Pittsburgh School of Medicine, Pittsburgh, PA 15261.

[4] Center for Discovery and Innovation, Hackensack Meridian Health, 111 Ideation Way, Nutley, NJ 07110, USA

[5] Department of Medical Sciences, Hackensack Meridian School of Medicine, Interprofessional Health Sciences Campus, 123 Metro Boulevard, Nutley, NJ 07110, USA

* Corresponding Author:

Denise E. Kirschner, Department of Microbiology and Immunology, University of Michigan Medical School, 1150 W Medical Center Drive, 5641 Medical Science II, Ann Arbor, MI 48109-5620, kirschne@umich.edu

Author summary

Tuberculosis (TB) is a top global health concern and treatment for TB requires multiple antibiotics taken for long periods of time, which is challenging for TB patients. Therefore, identifying regimens that are more effective and more patient-friendly than the standard treatment is urgently needed. It is also known that non-compliance leads to the development of drug resistant TB. In this work, we pair computational and experimental models to predict new regimens for the treatment of TB that optimize how fast bacteria are cleared using minimal dosage. We apply novel approaches to this goal and validate our predictions using a non-human primate model. Our findings suggest that systems pharmacological modeling should be employed as a method to narrow the design space for drug regimens for tuberculosis and other diseases as well.

Abstract

Tuberculosis (TB) continues to be one of the deadliest infectious diseases in the world, causing ~1.5 million deaths every year. The World Health Organization initiated an *End TB Strategy* that aims to reduce TB-related deaths in 2035 by 95%. Recent research goals have focused on discovering more effective and more patient-friendly antibiotic drug regimens to increase patient compliance and decrease emergence of resistant TB. Moxifloxacin is one promising antibiotic that may improve the current standard regimen by shortening treatment time. Clinical trials and *in vivo* mouse studies suggest that regimens containing moxifloxacin have better bactericidal activity. However, testing every possible combination regimen with moxifloxacin either *in vivo* or clinically is not feasible

due to experimental and clinical limitations. To identify better regimens more systematically, we simulated pharmacokinetics/pharmacodynamics of various regimens (with and without moxifloxacin) to evaluate efficacies, and then compared our predictions to both clinical trials and nonhuman primate studies performed herein. We used *GranSim*, our well-established hybrid agent-based model that simulates granuloma formation and antibiotic treatment, for this task. In addition, we established a multiple-objective optimization pipeline using *GranSim* to discover optimized regimens based on treatment objectives of interest, i.e., minimizing total drug dosage and lowering time needed to sterilize granulomas. Our approach can efficiently test many regimens and successfully identify optimal regimens to inform pre-clinical studies or clinical trials and ultimately accelerate the TB regimen discovery process.

Introduction

Tuberculosis (TB) is one of the deadliest infectious diseases in the world, with 1.6 million deaths in 2021 [1], and World Health Organization (WHO) aims to reduce the number of TB-related deaths by 95% by 2035 [1]. While vaccination efforts can reduce the number of new TB cases and deaths, a shorter but highly efficacious and safe drug regimen is needed to treat TB. Although new and efficacious drugs have been discovered for drug-resistant TB [2, 3], drug-susceptible TB disease has been treated with the same regimen for close to 50 years, namely 6-9 months of treatment with isoniazid (H), rifampin (R), ethambutol (E) and pyrazinamide (Z) [4]. Likely, changes to the existing standard regimen for drug-susceptible TB will help achieve WHO's goal.

Improving existing TB treatment involves finding regimens that account for the complexities of TB. The structure of the granuloma influences antibiotic distribution and can result in lower concentrations within granulomas [5-8]. Moreover, microenvironments within granulomas can promote the infecting bacteria, *Mycobacterium tuberculosis* (Mtb), to shift phenotypic states that are tolerant towards antibiotics [9-11]. Host-to-host variability in drug absorption and metabolism kinetics leads to pharmacokinetic (PK) variability that has been clinically linked to worse outcomes in TB treatment [12]. Furthermore, the lengthy treatment makes compliance challenging. While compliance yields high levels of success, intermittent treatment can lead to the development of drug resistance [13]. In short, by addressing these complications (heterogeneity in granulomas and antibiotic distribution, antibiotic-tolerant Mtb, host-to-host PK variability and long treatment times), a better regimen – one that would successfully treat more individuals with a shorter treatment duration – can be identified.

Due to these challenges, identifying new regimens for TB is a complex process that requires a combination of approaches to accurately capture different aspects of TB treatment [14]. Studies have classified the pharmacokinetic/ pharmacodynamic (PK/PD) features of individual TB antibiotics with *in vitro* methods, such as hollow fiber systems [15-17] and bactericidal assays in different growth conditions [18-20], and *in vivo* methods via HPLC coupled to tandem mass spectrometry (LC-MS/MS) and MALDI mass spectrometry imaging (MALDI-MSI) analyses [21-23]. However, these studies were mostly performed using single antibiotics and, due to heterogeneity among granulomas, variability of Mtb metabolic states and the propensity for Mtb to develop drug resistance, TB treatments with more than one antibiotic (i.e. combination therapy) are essential. To

quantify drug interactions and assess the efficacy of combination therapies, many studies have been performed: *in vitro* with checkerboard assays [24-26], *in vivo* with mouse [27, 28], using a non-human primate (NHP) animal models [29, 30], as well as *in silico* approaches applying machine learning algorithms [31, 32]. Moreover, many clinical studies have been performed with antibiotic combinations, which is crucial to assessing toxicity as well as long term outcomes of treatments [33-36]. These valuable studies are time-consuming and expensive, often prohibitively so.

Computational modeling can efficiently predict regimen efficacy and optimal doses, which is essential due to the high number of combinations of drug regimens in this large regimen design space (on the order of 10^{17} [37]). We have previously shown that our validated computational simulations of granuloma formation, function and treatment, called *GranSim,* can simulate efficacies of different TB regimens (c.f. [6, 8, 38]) and we can utilize surrogate-assisted optimization algorithms to accurately and efficiently predict optimal regimens [37].

Previous studies in murine models suggested that moxifloxacin (M) is a promising antibiotic to improve the standard regimen and decrease the duration of TB treatment due to its strong bactericidal activity [39-44]. To this end, a recent clinical trial, REMoxTB, attempted to shorten treatment from 6 months to 4 months by altering the standard HRZE regimen to HRZM or RMZE. However, the study failed to show noninferiority of moxifloxacin-containing regimens to the standard regimen due to higher relapse rates of these regimens [33]; after careful reanalysis, some patient populations were shown to be cured successfully with these moxifloxacin-containing regimens in a shorter treatment window [45]. In our study, we elaborate an approach toward identifying drug regimens

that are more effective in treating TB granulomas and that require shorter treatment times compared to the standard regimen. We used our computational model *GranSim* to create an *in silico* biorepository of hundreds of granulomas, combined with *in vivo* data generated from a NHP model and applied a surrogate-assisted optimization algorithm to identify regimen success and failure. We first simulated moxifloxacin-containing regimens using *GranSim* and identified regimens that are superior to the standard treatment based on sterilization times. Informed by our simulation results, we performed an *in vivo* study in NHPs to test our predicted regimens that haven't been studied before, validating our simulation predictions. Thus, our study identifies new regimens that can inform pre-clinical trials to shorten treatment times and minimize dosages. This highlights the importance of using modeling prior to pre-clinical trials as a step towards a more efficient and directed regimen design for TB.

Results

In silico library of granulomas for treatment simulations and dose optimization

We first generated an *in silico* library of 750 granulomas over 300 days that matches NHP dataset of 600 granulomas [46, 47]. To do that, we sampled 250 granuloma parameter sets within biological feasible ranges using the LHS method and simulating three replications with each parameter set to capture both types of uncertainty present [48]. We then classified granulomas that have nonzero bacterial loads (those that did not sterilize) by measuring their colony forming units (CFUs) as either *low-CFU* or *high-CFU granulomas*, depending on their CFU trends (Fig 1) In this work, we simulated different treatments on subsets of granulomas from this library of both high- and low-CFU

granulomas as well as combined. This follows as humans and NHPs have multiple granulomas within their lungs, and ensures that we test each regimen on a variety of granuloma types and multiple granulomas, making it relevant to both experimental data and clinical TB outcomes. Here, low-CFU granulomas represent the state where the immune system controls bacterial growth within a granuloma, whereas within high-CFU granulomas, bacteria grow to large numbers and can disseminate [8, 49, 50]. Specifically, if the number of CFUs within a granuloma is less than 10^4 at the end of the simulation and has not increased more than 50 CFUs in the last 20 days of simulation, we label it as a *low-CFU granuloma* (Fig 1, blue curves). If the number of CFUs in a granuloma is between 10^4 and 10^7 at the end of the simulation or it has increased by more than 50 CFUs in the last 20 days of simulation, we label it as a *high-CFU granuloma (*Fig 1, red curves). We proposed 10^4 CFUs/granuloma as a threshold for low-CFU granulomas, based on the observed CFU trends of the 750 granulomas we simulated: granulomas with CFUs lower than this threshold tend to stabilize in our simulations (Fig 1, blue curves), representing controlled growth. However, granulomas with CFUs higher than this threshold tend to grow uncontrollably (Fig 1, red curves). We can alter this threshold without loss of generality.

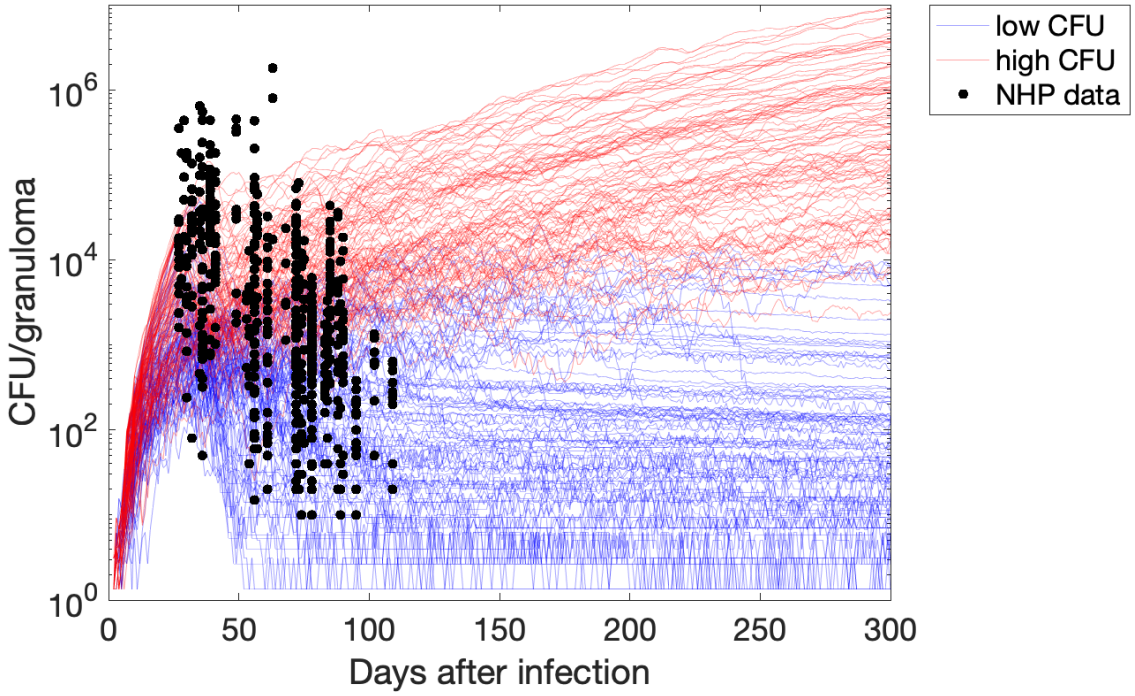

Fig 1. CFU trends within the *in silico* repository of simulated granuloma generated by *GranSim* after the start of infection. Each curve represents a single granuloma simulation with a single parameter set using *GranSim,* and black dots are data from NHP studies [46, 47]. Based on their CFU trajectories, we categorize granulomas into low-CFU (blue curves) and high-CFU (red curves) granulomas. Low-CFU granulomas represent granulomas that have controlled bacterial burden; high-CFU granulomas are those where bacterial growth is uncontrollable by the immune system, respectively [8, 49, 50].

Simulations capture the rapid rate of sterilization with moxifloxacin-containing regimens that is observed in clinical trials

We first compare the standard regimen for TB, i.e., HRZE, with various moxifloxacin-containing regimens. A recent clinical trial (REMoxTB) compared the 6-month standard regimen HRZE treatment (control group) to 4-month treatment with two moxifloxacin-containing regimens, HRZM (termed the “isoniazid group” in the original study) and RMZE (termed the “ethambutol group” in the original study) (see Table 1 for the protocol) [33]. Regimens with moxifloxacin were not found to be suitable replacements for the standard regimen, as they had a higher rate of relapse in patients after the end of treatment, even

171 though they decreased the bacterial load in patients' sputum more rapidly at the beginning
172 of the treatment (Fig 2A).

173

174 **Table 1. Simulation protocols used in this study.** Those indicated as clinical trial correspond to the
175 regimens used in [33], and those indicated as NHP study correspond to the regimens tested in NHPs herein.
176 HRZEM combinations refer solely to the computational studies. Optimization refers to the regimens we
177 further tested with our optimization protocol to determine dosing and sterilization time to predict the best
178 performers.

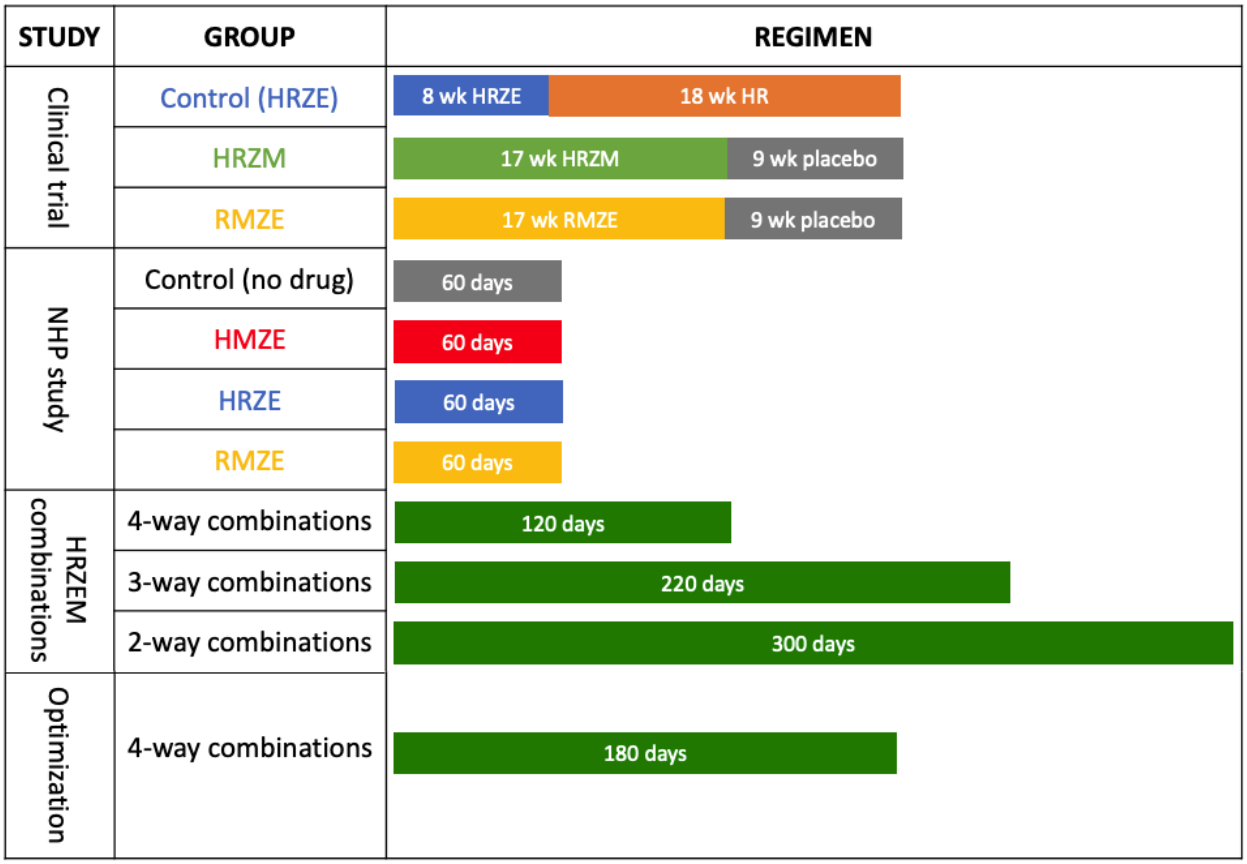

179

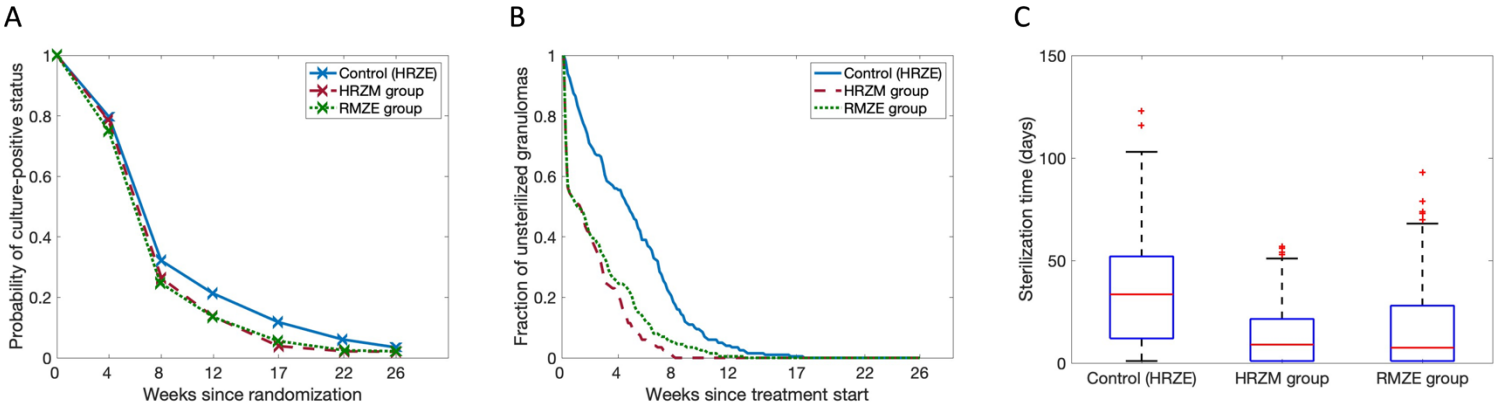

Fig 2. Comparison of moxifloxacin-containing regimens to the standard regimen for the human study and *GranSim*. (A) Results from the REMoxTB clinical trial [33]. Probability that a patient has a sputum culture-positive status decreases over the course of treatment, and this decline is more pronounced for moxifloxacin-containing regimens. Control (HRZE), HRZM and RMZE groups have 510, 514 and 524 patients, respectively. This figure is adapted from Fig 2B of [33] (Data points (x) extracted by WebPlotDigitizer). (B,C) *GranSim* predictions for (B) the fraction of unsterilized granulomas and (C) average sterilization times upon treatment with HRZE, HRZM and RMZE (*p<0.001, one-tailed paired t-test). For the REMoxTB study and the simulations, in the control groups, patients/granulomas are treated with HRZE for 8 weeks, followed by an 18-week long HR treatment. In HRZM and RMZE groups, patients/granulomas are treated with HRZM and RMZE for 17 weeks, respectively (see Methods and Table 1). In (B) and (C), each group has 200 simulated granulomas.

We used *GranSim* to simulate the same protocol as in the REMoxTB study (see Methods and Table 1). Our results agree with the clinical trial: moxifloxacin-containing regimens reduced the bacterial load faster, as ~40% of the granulomas were sterilized within the first week (Fig 2B, dashed red and dotted green curves). By comparison, the standard regimen required more than 4 weeks to sterilize the same number of granulomas (Fig 2B, blue curve). To treat the whole set of granulomas successfully (i.e., both low-and high-CFU), HRZE, HRZM and RMZE-treated groups need 17, 8 and 12 weeks of treatment, respectively. The metric “average time to sterilize a granuloma” follows a similar trend: HRZM-treated group has the shortest average sterilization time with ~14 days, followed by RMZE- (~17 days) and HRZE-treated (~35 days) groups. Therefore, our simulations suggest that the HRZM is the most effective regimen in terms

of bactericidal activity, followed by RMZE, although the difference between these two regimens is minimal yet significant ($p<0.001$). The control group, HRZE, is the slowest to sterilize granulomas.

Regimens HMZE, HRZE and RMZE reduce bacterial burden in both NHP studies and simulations

NHPs with active TB were treated with the TB standard regimen HRZE as well as two moxifloxacin-containing regimens: RMZE and HMZE (see Table 1 and Methods). Daily administration of drugs was initiated at 13 weeks post-infection and continued for 8 weeks at which time the macaques were necropsied. Total CFU was calculated by summing the CFU counts obtained from plating multiple tissue samples (lung, granulomas, LNs) from each animal. Each regimen was able to reduce bacterial burden in NHPs compared to controls (Fig 3D and E). Simulations with *GranSim* indicated that moxifloxacin-containing regimens, HMZE and RMZE, sterilize more granulomas in a shorter time frame than the standard regimen, HRZE (Fig 3A-C).

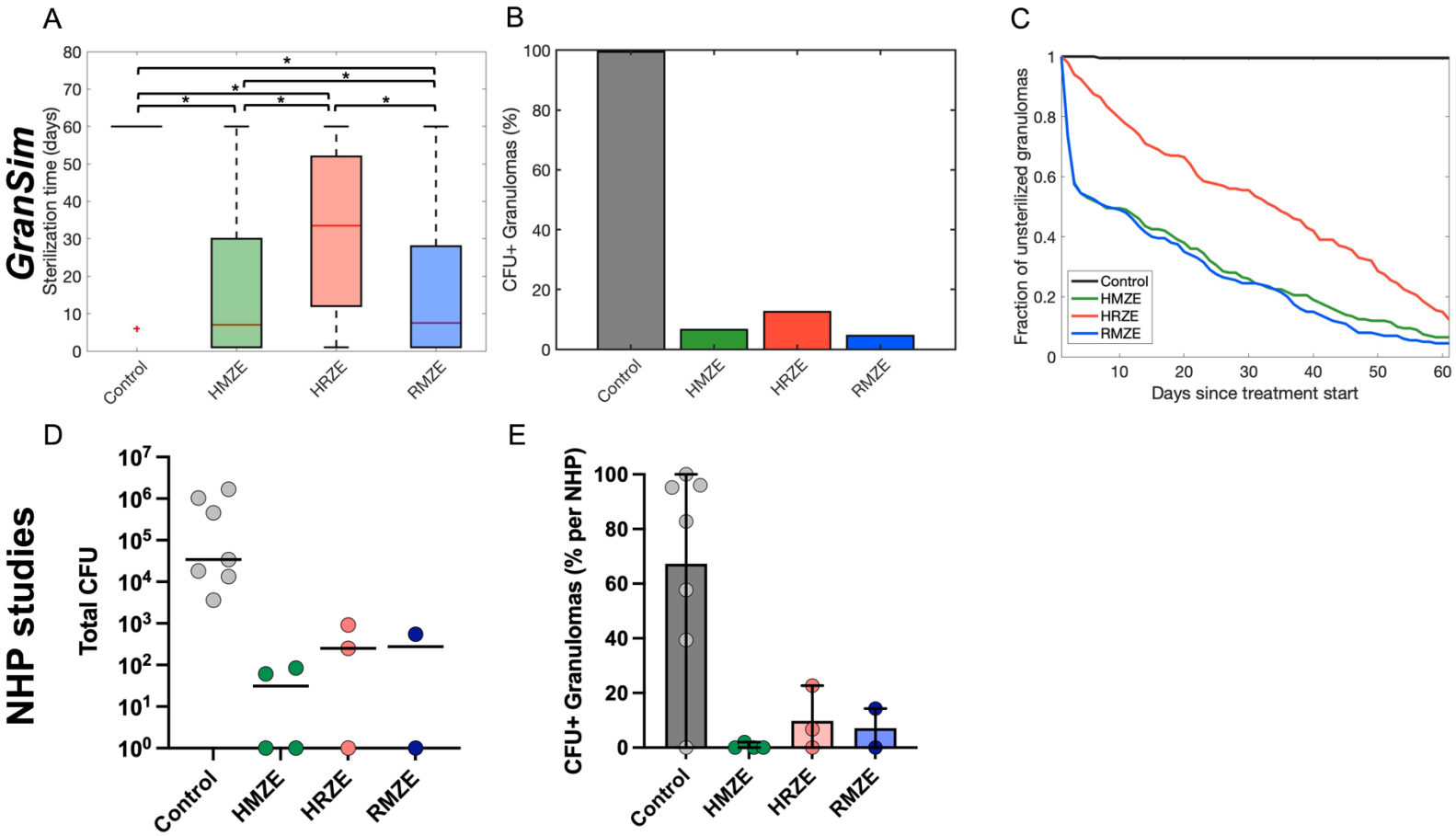

Fig 3. Comparing NHP and *GranSim* regimens. Comparison of the standard regimen (HRZE) to two moxifloxacin-containing regimens, HMZE and RMZE, between *in silico* studies with *GranSim* (panels A-C) and *in vivo* NHP studies (panels D and E). (A) The sterilization times of granulomas averaged over 200 granulomas in *GranSim*. Note that we assign the maximum simulation time of 60 days as a sterilization time for unsterilized granulomas (*p<0.001, one-tailed paired t-test). (B, E) Percentage of granulomas that are unsterilized by treatment end for (B) NHP studies and (E) *GranSim*. Colored dots in (E) represent the percentage of unsterilized granulomas per NHP. (C) The fraction of granulomas which are unsterilized as a function of simulated treatment time using *GranSim.* (D) The average total CFU per NHP after treatment with the corresponding regimens for two months (n=7 animals in the control group, n=3 animals in HRZE group, n=4 animals in HMZE, n=2 animals in RMZE). Statistical analyses were not performed on the NHP data due to small numbers of animals per group.

Metabolic activity within granulomas is decreased with antibiotic treatment in both NHPs and simulations

We used PET-CT imaging on NHPs with FDG uptake to assess how drug regimens influence inflammatory activity of granulomas. We measured standardized uptake value

ratio (SUVR), a previously developed measure to quantify the FDG avidity per granuloma [30, 51]. Treatment with HRZE or HMZE reduced FDG avidity of granulomas within 8 weeks, whereas there was no change in FDG avidity in response to RMZE treatment, similar to that of the control group (Fig 4A). In *GranSim*, we can monitor metabolic activity of a granuloma based on the number of various cell types and inflammatory measures of activity within granulomas (see Methods for more details). Similar to the FDG PET-CT results from NHP experiments, *GranSim* simulations demonstrated that all treatment regimens decrease metabolic activity significantly (Fig 4B).

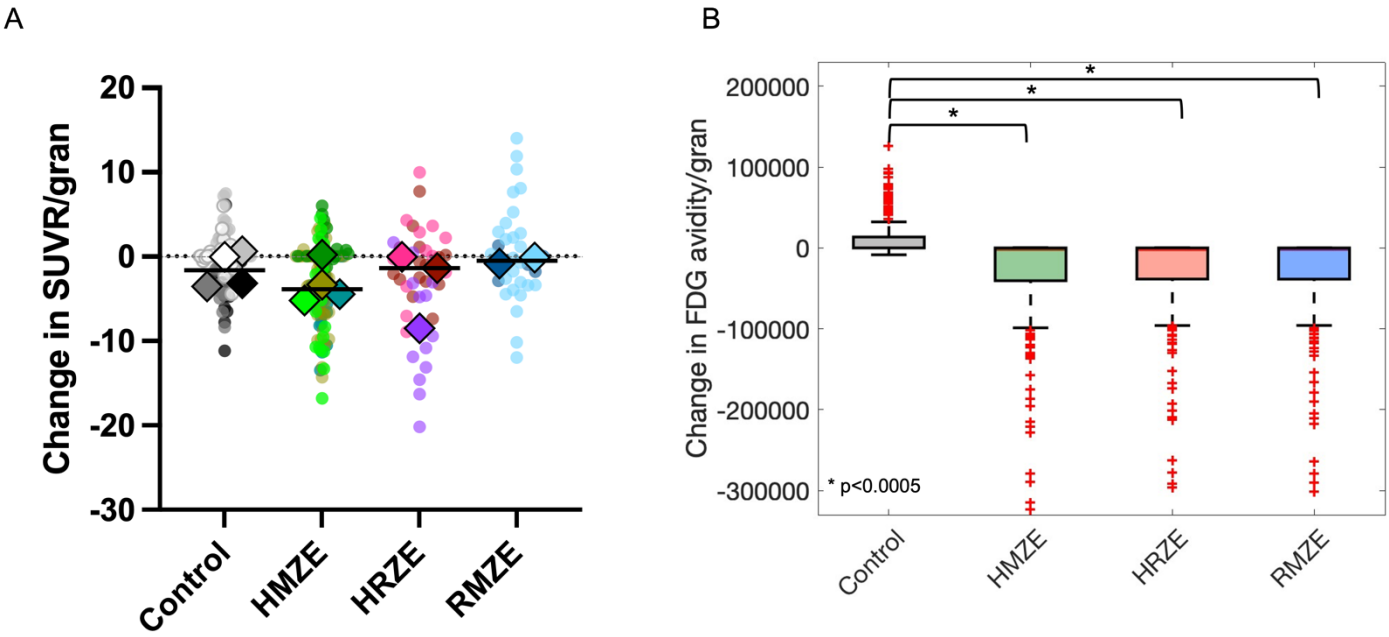

Fig 4. Comparison of metabolic activity (measured by SUVR) change post treatment in NHP and *GranSim*. Comparison of metabolic activity changes (A) in NHP granulomas and (B) using *GranSim*. (A) Change in standardized uptake value ratio (SUVR) per NHP granuloma (colored dots) in 8 weeks ($SUVR_{8weeks}$ - $SUVR_{pre\text{-}treatment}$) when NHP are treated with HRZE (n=3 animals), HMZE (n=4 animals) and RMZE (n=2 animals) for 8 weeks (n=7 animals in control case, i.e., without treatment). Color shades of the dots in each column indicate NHPs and the diamonds are the median of SUVR change/granuloma for each NHP. (B) Change in FDG avidity per granuloma simulated using *GranSim* (FDG $avidity_{8weeks}$ - FDG $avidity_{pretreatment}$) averaged over 200 granulomas (*p<0.0005, one-tailed paired t-test).

Simulations reveal that moxifloxacin-containing regimens have a better bactericidal activity than HRZE

To systematically compare the efficacy of moxifloxacin-containing regimens to the standard regimen, we used *GranSim* to simulate treatment with all 4-way combinations of HRZEM (HRZE, RMZE, HMZE, HRME and HRZM) for 120 days (Fig 5). We analyze simulation results distinguishing granulomas that are high-CFU (Fig 5A and D) versus low-CFU (Fig 5B and E), as well as combined (Fig 5C and F). Our simulation results indicate that all four regimens containing moxifloxacin clear Mtb within all types of granulomas (high-CFU, low-CFU, and combinations) in a shorter time than the standard regimen HRZE (blue curve in Fig 5A-C, gray box in Fig 5D-F). Moreover, simulations show that the initial decline in bacterial load for combinations of high- and low-CFU granulomas with regimens containing moxifloxacin (Fig 5C) stems from the fast sterilization of all low-CFU granulomas (Fig 5B), as the clearance rate for high-CFU granulomas is slower than that for low-CFU granulomas. In addition, the differences between various moxifloxacin-containing regimens are more pronounced in high-CFU granulomas. For example, HRZM clears all high-CFU granulomas by 51 days, which is the fastest of all 4-way combinations of HRZEM. The next best regimen is HRME, requiring 77 days to sterilize all granulomas with high-CFU. RMZE and HRZE sterilize all high-CFU granulomas by a similar time window, in 94 and 97 days, respectively. Lastly, treating all granulomas until they sterilize with HMZE takes 118 days. However, the average time required to sterilize a high-CFU granuloma (Fig 5D) is lower for moxifloxacin-containing regimens (Fig 5D, red boxes) than that for the standard regimen (Fig 5D, black box), which is consistent with the findings in Figs 2-3.

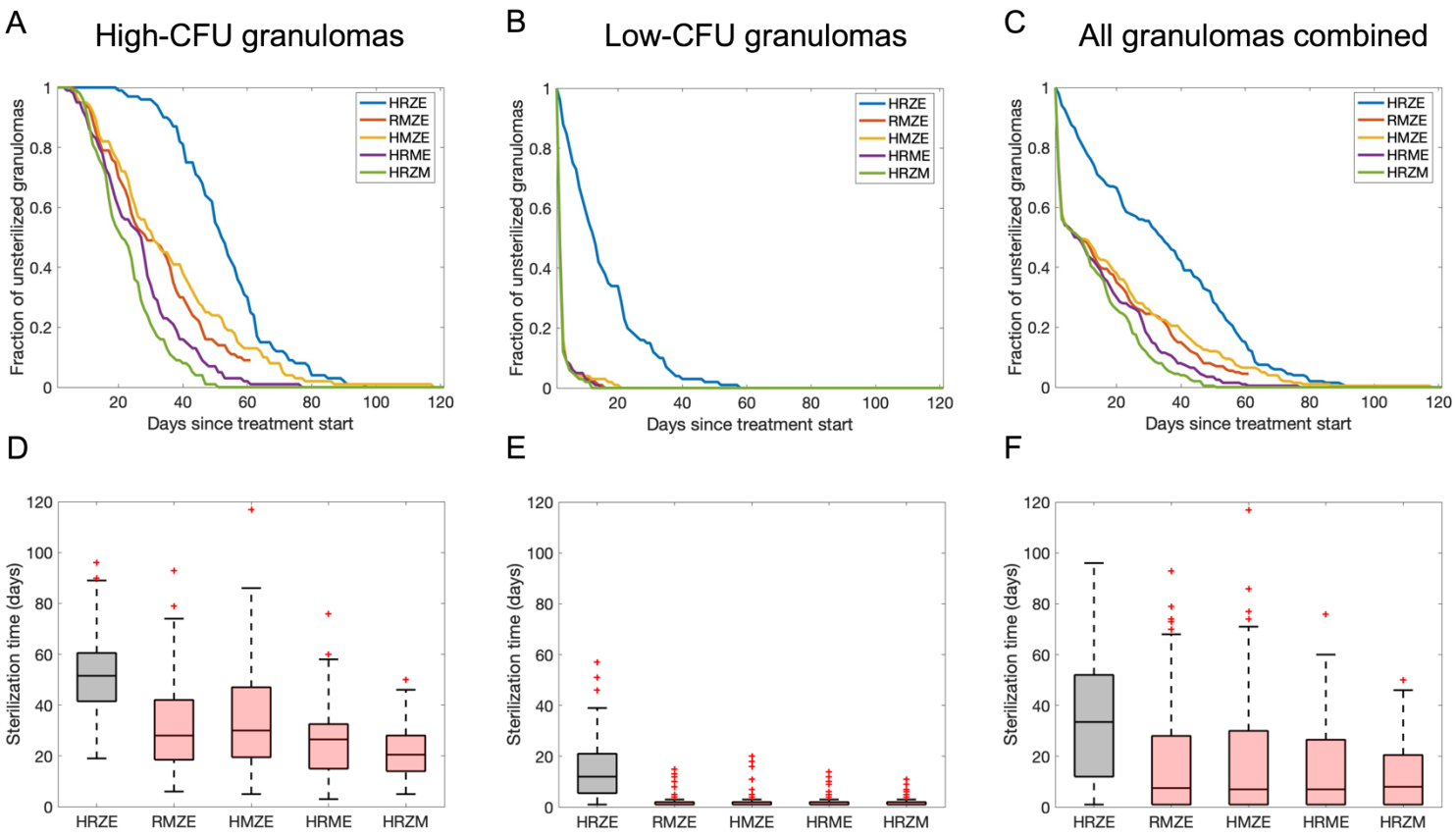

278

279 **Fig 5. Comparison of 200 simulations for all HRZEM four-way regimens using *GranSim*.** Comparison
280 of (A-C) sterilizing rates and (D-F) average sterilization times of 4-way combinations of HRZEM for (A and
281 D) 100 high-CFU, (B and E) 100 low-CFU and (C and F) a combination of 100 high- and 100 low-CFU
282 granulomas.
283

284 **Simulations show that moxifloxacin-containing regimens are more efficacious than**
285 **HRZE with fewer than four antibiotics**

286 Compliance is one of the challenges of TB treatment due to the long-term use of many
287 antibiotics with numerous side effects. To identify a more patient-friendly treatment, in line
288 with the goals of the END TB strategy of WHO [52], we could reduce the number of
289 antibiotics used in a regimen and/or reduce the total dose of a regimen. To test whether
290 a regimen with fewer than four antibiotics would be as efficient as (or more efficient than)
291 the 4-way combinations of HRZEM, we simulated all 3-way (S3 Fig) and 2-way (S4 Fig)

292 combinations of HRZEM in treating individual granulomas. As compared with 4-way
293 combinations (Fig 5B and E), we also observed the fast clearance of low-CFU
294 granulomas treated with moxifloxacin-containing regimens in 3- (S3B Fig and S3E Fig)
295 and 2-way (S4B Fig and S4E Fig) combinations. Sterilization of high-CFU granulomas
296 remains faster with 3-way combinations containing moxifloxacin than for regimens without
297 moxifloxacin; however, the rate of sterilization is slower than for low-CFU granulomas
298 (S3B Fig and S3E Fig). The trend does not always hold for treatment of high-CFU
299 granulomas with 2-way combinations containing moxifloxacin (S4B Fig and S4E Fig).
300 Regimens like ZM and EM cannot sterilize most of the high-CFU granulomas despite
301 prolonged treatment (S4B Fig). These granulomas may be related to the classically
302 defined paucibacillary granulomas which even after treatment remain difficult to sterilize
303 [53].

304 Lastly, we compared treatments with all 2-way, 3-way and 4-way combinations of
305 HRZEM to the standard regimen HRZE based on the average sterilization time for each
306 regimen of high-CFU (Fig 6A) and low-CFU (Fig 6B) granulomas and both types of
307 granulomas combined (Fig 6C). Our results demonstrate that regimens that are more
308 effective in sterilizing granulomas than HRZE each contain moxifloxacin (colored curves
309 in Fig 6). For high-CFU granulomas, a moxifloxacin-containing regimen with at least 3
310 antibiotics is needed to achieve a better performance than HRZE (Fig 6A). However,
311 sterilizing low-CFU granulomas faster than HRZE is possible even with regimens
312 containing two antibiotics (HM, RM and ZM in Fig 6B). These comparisons are based
313 only on the standard doses of regimens; optimization of doses is also possible.

314

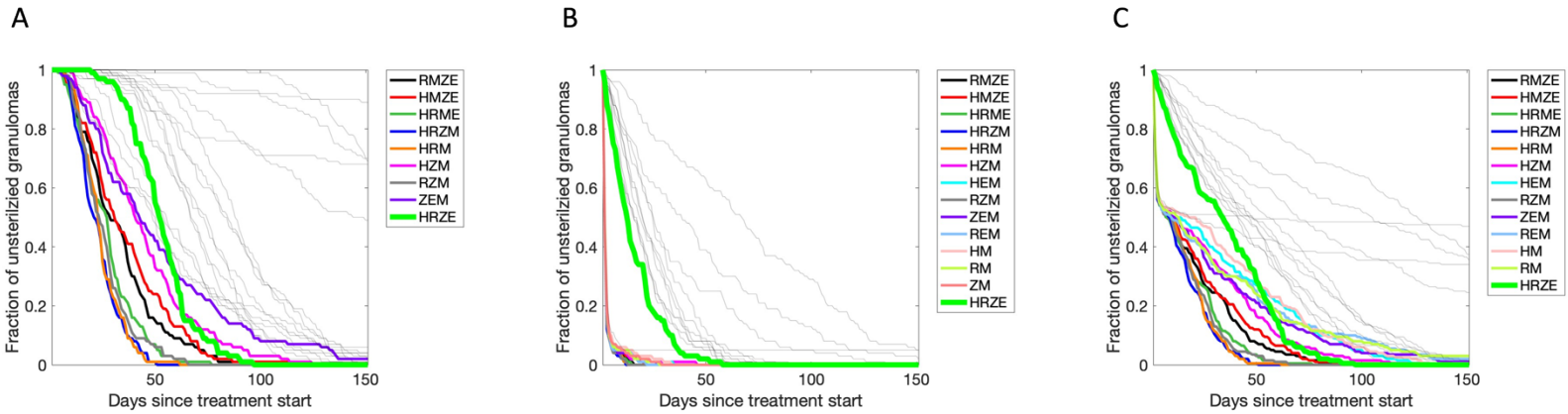

315 **Fig 6**. **Simulated treatments with 4-way, 3-way, 2-way regimen comparison from HRZEM.** Visually
316 comparing all regimen combinations to HRZE (thick green curve in all panels) in (A) high-CFU, (B) low-
317 CFU and (C) all granulomas (high- and low-CFU granulomas combined). Colored curves indicate the
318 regimens that clear granulomas faster than HRZE, i.e., they have a lower average sterilization time
319 averaged over 100 simulations (200 simulations in (C)). Gray curves represent regimens with slower
320 sterilization.

321

322 **Dosing optimization method identifies new doses for regimens**

Optimizing the dose of each antibiotic in all 4-way combinations of HRZEM may reduce the total antibiotic dose, contributing to our goal of a more patient-friendly TB treatment. Here, we use Pareto optimization to predict optimal solutions that balance the trade-off between two treatment objectives: minimizing the total antibiotic dose and minimizing the average time for regimens required to sterilize all Mtb within granulomas, i.e., the *average sterilization time*. Based on these two objectives, our Pareto optimization pipeline predicts the Pareto front for each 4-way combination regimen of HRZEM (HRZM, HRME, HMZE, RMZE and HRZE) and outputs a set of optimized regimens that belong to the Pareto set (i.e., optimal doses) (Fig 7A-E, red dots).

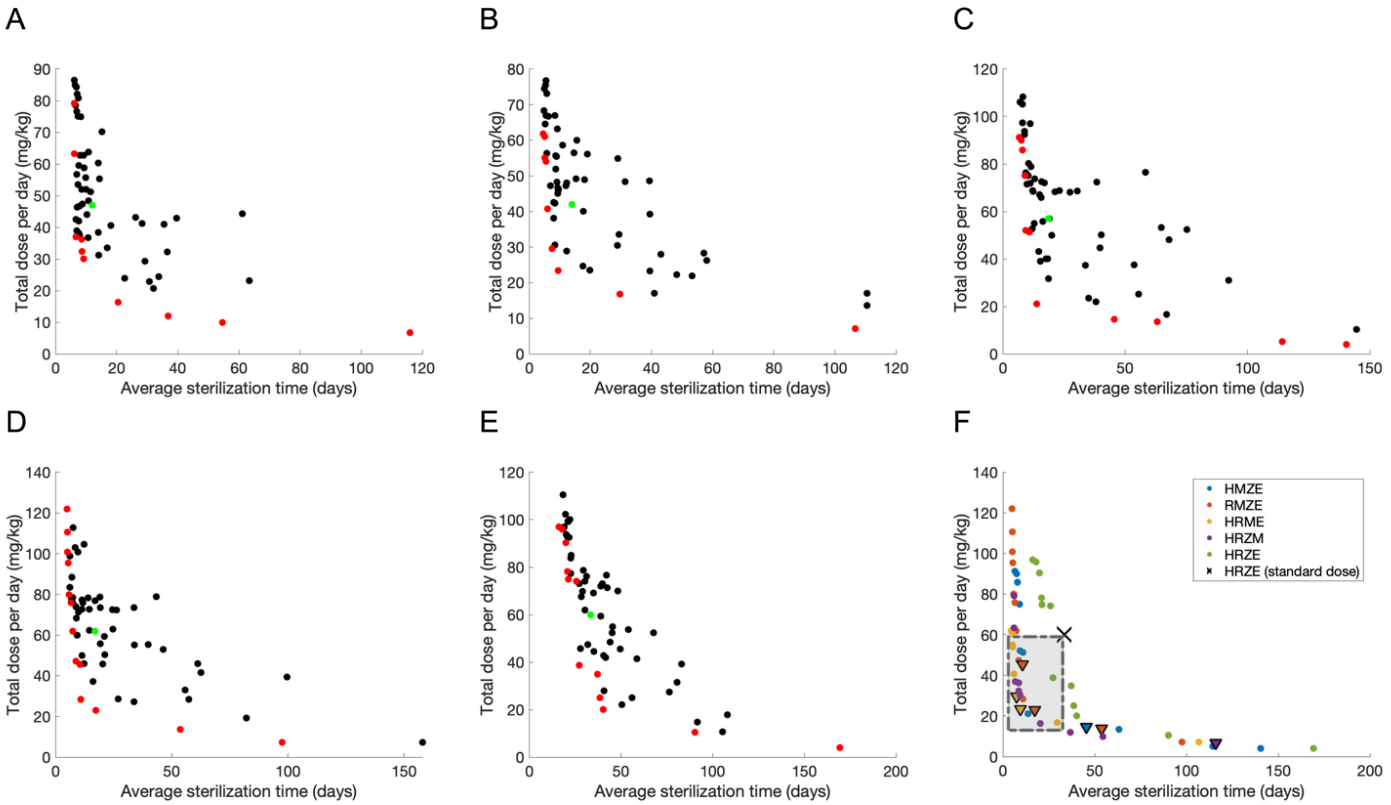

Fig 7. Pareto front optimization study simulating all 4-way combinations of HRZEM to find regimens that minimize both average sterilization time and total dose. Pareto front optimization identifying optimal dose and sterilization times for: (A) HRZM, (B) HRME, (C) HMZE, (D) RMZE and (E) HRZE. In each panel (A-E), red dots represent the (non-dominating) regimens that belong to the Pareto set (see S2-6 Tables for the doses of each antibiotic in the regimens that belong to Pareto sets) whereas black dots are the regimens that are not optimal based on the objectives. Green dots show the regimen based on the current standard doses recommended by CDC [4]. (F) Pareto sets for all regimens (same as red dots in

339 panels A-E) compared to the standard regimen HRZE with CDC-recommended doses (**X** in Panel F). Dots
340 in the dashed gray rectangle indicate the regimens that have lower total drug dose and lower average
341 sterilization times (see Table 2 for the doses of each antibiotic in these regimens). Triangles indicate
342 optimized regimens with 3-way combinations, as the optimal doses of one antibiotic (E or Z) in these
343 regimens are predicted as 0.
344

345 In general, regimens that simulations identify as optimal (i.e., regimens in the
346 Pareto set) span a wide range of total dose and average sterilization times. This suggests
347 that among optimized regimens, some have very low average sterilization times at the
348 cost of a very high antibiotic dose and some regimens have a very low total dose leading
349 to long sterilization times. However, we are particularly interested in optimized regimens
350 that have both lower total dose and lower average sterilization times as compared to
351 standard regimen (HRZE with CDC-recommended doses). Our method predicts that the
352 19 regimens in the dashed gray rectangle (Fig 7F) are all more advantageous than the
353 standard regimen (black dot in Fig 7F) in terms of reducing *both* total dose and sterilization
354 time. These regimens tend to have higher doses of rifampicin than the standard regimen
355 yet lower total regimen dose (Table 2), resulting in shorter sterilization times, which is in
356 line with clinical trials that showed a reduction in time to culture conversion using higher
357 doses of rifampicin [54, 55]. Based on our earlier results, it is not surprising that these
358 optimized regimens mostly contain moxifloxacin (Table 2). This is also expected based
359 on clinical studies where moxifloxacin-containing regimens sterilize granulomas more
360 efficiently (c.f. Fig 2). Further, although most of these optimal regimens contain four
361 antibiotics, our pipeline also predicted a few optimal combinations with less than four
362 antibiotics (see triangles in the rectangle region of Fig 7F; rows labeled with triangles in
363 Table 2). (Our pipeline predicts the ethambutol optimal dose as 0 for HRME and RMZE
364 regimens and the pyrazinamide optimal dose as 0 for RMZE, thus identifying HRM, RMZ

and REM as additional optimal regimens). This agrees with our systematic study of all possible combinations that determined HRM, RZM and REM as more efficient regimens than the standard regimen HRZE (c.f. Fig 6). Our optimization approach provides a more efficient way to identify regimens with different combinations of antibiotics than is possible in clinical or experimental studies.

Table 2. Simulated Doses of Antibiotics that optimize treatment objectives (compare with Fig 7). The doses for each antibiotic in the regimens that have lower average sterilization time and lower dosage than the standard regimen (black row) as shown in Fig 7F (i.e., all regimens in dashed gray rectangle). Optimized doses for HMZE, RMZE, HRME, HRZM and HRZE are color-coded as blue, brown, yellow, purple and green, respectively. The rows labeled with a triangle indicate optimal 3-way combinations, where the optimal dose of E or Z is predicted as 0.

Avg Sterilization Time (days)	Total dose (mg/kg)	H	R	Z	E	M
33.6	60	5	10	25	20	0
5.1	55.2	6.1	20.0	0	16.8	12.3
5.5	53.4	7.5	13.9	0	19.7	12.3
6.1	40.8	9.0	11.3	0	7.2	13.3
6.7	37.0	8.8	19.7	0.6	0	7.9
▼7.5	29.6	5.5	10.1	0	0	14.0
8.6	36.4	1.3	16.0	9.0	0	10.1
8.7	32.3	8.7	7.7	5.1	0	10.8
8.8	47.2	0	18.4	16.0	4.1	8.7
9.2	30.1	10	9.7	3.9	0	6.5
9.3	52.2	8.7	0	31.2	0.5	11.8

9.5	23.4	6.7	9.2	0	0	7.5
10.6	45.4	0	9.2	26.9	0	9.3
10.9	51.3	9.8	0	18.7	12.9	9.9
11.0	28.4	0	13.3	2.6	1.0	11.5
13.8	21.1	8.2	0	2.6	1.0	9.3
17.3	23.0	0	12.7	0	2.5	7.8
20.5	16.4	9.1	0.9	1.2	0	5.2
27.3	38.7	4.7	19.0	14.2	0.8	0
29.7	16.8	5.4	5.1	0	3.1	3.2

Discussion

One of the strategies to improve TB treatment regimens is to shorten treatment duration by introducing or substituting newer antibiotics that have better bactericidal activities than those in the current standard regimen (HRZE), for example, by considering bedaquiline, pretomanid, linezolid [56] or moxifloxacin [33]. To this end, clinical trials [33, 41, 43] and also *in vivo* studies with mice [39, 40, 44] have been conducted to explore a moxifloxacin-containing regimen that decreases treatment duration. In this study, we employ three unique approaches to predict more patient-friendly treatment regimens for TB: replacing antibiotics in the standard regimen with moxifloxacin *in vivo* and *in silico*, reducing the

386 total number of antibiotics in a regimen by scanning all regimen combinations *in silic*o,
387 and reducing the total dosage using an *in silico* drug optimization pipeline.

388 Previously, we explored regimens with and without moxifloxacin in our simulation
389 framework, *GranSim,* to compare with early-phase clinical trials [57]. However, this is the
390 first study that directly compares TB treatment simulations using *GranSim* to a phase 3
391 clinical trial (REMoxTB [33]) (Fig 2). We also perform NHP studies with promising
392 regimens predicted by *GranSim*. (Figs 3 and 4). Different from our previous studies, we
393 systematically analyzed all possible combinations with or without moxifloxacin and
394 employed a new optimization pipeline to identify optimal regimens that sterilize
395 granulomas more efficiently than HRZE.

396 Previous clinical trials concluded that both 4 months of HRZM treatment and 4
397 months of RMZE had better bactericidal activity than the control group (HRZE) based on
398 the conversion to culture negativity status of the patients (Fig 2A) [33]. In our simulations,
399 we observe a similar trend as in the clinical trial in terms of bactericidal activity: HRZM
400 and RMZE groups are more effective in reducing bacterial load and sterilizing granulomas
401 than the control group (Fig 2B and C). Although the measures of the clinical trial and our
402 simulations are at different scales (host-scale measures in clinical trials and granuloma-
403 scale measures in simulations), both studies support that moxifloxacin is a promising
404 regimen.

405 NHP experiments with standard and moxifloxacin-containing regimens indicate
406 that all regimens reduce the total CFU of NHPs (Fig 3D) by sterilizing the majority of NHP
407 granulomas (Fig 3E and S5 Fig). Furthermore, granuloma metabolic activity (surrogate
408 for inflammation) drops by treatment with HRZE and HMZE only, while RMZE does not

affect the metabolic activity. These outcomes are in agreement with our simulations; however, simulations predict that RMZE is equally effective as HMZE in sterilizing granulomas and reduces metabolic activity. This difference may stem from the small sample size in NHP studies but likely also is due to *in vivo* factors that are not included within *GranSim*. In addition, the surrogate measures used for FDG avidity in granulomas are only an approximation of the factors involved in *in vivo* FDG avidity. Using *GranSim*, we simulated 200 distinct granulomas per regimen. However, due to resource limitations, sample sizes were necessarily smaller in the NHP studies, and RMZE has the smallest sample size with only 2 animals. Moreover, unlike *in silico* studies where we simulate treatment with the same set of granulomas over various regimens, *in vivo* studies require different sets of animals to test regimens, and the outbred nature of macaques adds another level of variability, although this is also true in humans.

To test the efficacy of moxifloxacin-containing regimens more systematically and to potentially reduce the number of antibiotics needed per regimen, we simulated the treatment of low- and high-CFU granulomas with all 4-way (Fig 5), 3-way (S3 Fig) and 2-way (S4 Fig) combinations of HRZEM. In this study, we conclude that any 4-way, 3-way or 2-way (except EM) combinations that include moxifloxacin are more efficacious in eliminating bacteria within low-CFU granulomas than HRZE (Fig 6B). However, only 4-way combinations and some of the 3-way combinations work better than HRZE for treating high-CFU granulomas (Fig 6A). This suggests that decreasing the number of antibiotics within a regimen may be challenging when treating more progressive, caseous granulomas with the 5 drugs in this study, whereas granulomas with lower CFU numbers are easier to treat with fewer antibiotics.

Most of the regimens that are 2-, 3- or 4-way combinations of HRZEM consistently decrease the fraction of granulomas remaining unsterilized over the course of the treatment and, subsequently, clear them all (Fig 5A-C, S3A-C Fig, S4A-C Fig). However, some regimens cannot sterilize further, i.e., fraction of unsterilized granulomas stays the same over a prolonged treatment time, (especially high-CFU granulomas). This may follow as high-CFU granulomas are mainly caseous with bacteria trapped within that region. It is known that moxifloxacin does not homogeneously diffuse into the caseous core of granulomas [5, 58]. Therefore, a regimen containing moxifloxacin needs to be complemented with antibiotics that are effective in killing Mtb trapped within caseum of granulomas, unlike ethambutol (E) [59, 60] or pyrazinamide (Z) [20, 59]. Treatment of high-CFU granulomas with ZM or EM decreases the bacterial load initially, but eventually results in granulomas with primarily Mtb in caseum (S6 Fig) that could not be sterilized by prolonged treatments with ZM (S6A Fig) or EM (S6B Fig). This suggests that ZM or EM treatments may result in granulomas that harbor bacteria that could later lead to relapse disease [61]. Although treatment with EM or ZM could not sterilize all high-CFU granulomas, 20% and 40% of high-CFU granulomas are cleared by EM and ZM treatment, respectively (S4A Fig).

Another novel approach introduced in this study is implementing an optimization pipeline into *GranSim* to optimize doses of the drugs within regimens using a multi-objective optimization algorithm. Previously, we studied optimization in *GranSim* by comparing genetic algorithm and radial basis function (RBF) network surrogate models and showed that using an RBF network method is more efficient in optimizing drug regimens without losing accuracy [37]. However, the RBF network method is based on

minimizing one objective function that may consist of various weighted terms, depending on the objectives we consider in order to discover a better regimen. A Pareto set is a set of solutions that is used to minimize multiple objectives with varying levels of importance. Therefore, determining the Pareto front with a single objective function would require many iterations of optimization to obtain a wide-ranging Pareto set [62]. Thus, multi-objective Pareto optimization is a more efficient approach to discover the optimal solution set.

To successfully optimize the doses of a regimen, it is crucial to have well defined objectives based on the factors that we would like to consider in a regimen. In this study, we assumed that the total dosage of a regimen, independent of the antibiotic, should be minimal. Moreover, the regimen should sterilize granulomas as quickly as possible. However, we can modify these objectives or add additional ones to obtain more biologically relevant optimized regimens. For instance, each antibiotic has different levels of adverse side effects and high doses should be avoided. Moreover, financial burden of each regimen should also be considered in order to identify more accessible treatments worldwide.

Computational modeling studies have many advantages that are useful for drug discovery studies and that complement experimental studies. Unlike clinical trials and *in vivo* experiments, our computational approach has the power to evaluate the efficacy of regimens o*n the same set of granulomas to eliminate the variability*. Moreover, due to limited resources, trying every single regimen combination *in vivo* experimentally or clinically, or repeating the experiment many times to achieve significance may not be feasible. Hence, promising regimens may be skipped or missed due to nonsignificant

478 results. Here, we predicted new and promising combination regimens that have not yet
479 been studied clinically, such as HMZE that informed our NHP studies and was predicted
480 to be an effective regimen via our simulations. Another drawback of clinical and *in vivo*
481 studies is the risk of disease relapse. To assess the relapse rate after treatment, study
482 subjects are observed for several months. Unlike experiments, we can track each Mtb
483 bacilli in our simulations that gives us the power to anticipate relapse at the end of the
484 treatment based on the sterilization status. Having unsterilized granulomas at the end of
485 treatment is predictive of TB relapse.

486 One limitation of our approach is that our model is at granuloma-scale. However,
487 predicting the relapse rates requires a host-scale model. Additionally being able to treat
488 a collection of granulomas within a host can serve to elaborate further the studies herein.
489 The source of relapse is not fully understood. One hypothesis suggests that bacteria
490 within granulomas in lymph nodes could migrate to the lungs and induce reinfection or
491 reactivation [63]. Therefore, a host-scale immune model of TB that contains multiple
492 granulomas within lungs and lymph nodes is needed to assess regimens' long-term
493 efficacy and to determine relapse rates, which are crucial parameters to evaluate
494 regimens efficiently, and we are currently adapting our host-scale TB model, *HostSim* [46,
495 64], to encompass antibiotics and meet this need. These next-generation improvements
496 will make our approach more powerful and reliable, so that *in vivo* experiments or clinical
497 trials can be systematically informed by simulation results.
498

499 # Methods

We combined computational modeling with studies in NHPs, outlining the approaches for each below. We point out where modifications to existing protocols and models have changed in the next-generation versions used herein.

GranSim

As a basis for studying treatment at the granuloma scale, we used our well-established computational model of granuloma formation and function, *GranSim*. *GranSim* is a hybrid agent-based model (ABM) that simulates the immune response during Mtb infection, capturing granuloma formation as an emergent behavior [6, 65-68]. Agents in this ABM include immune cells, such as macrophages and T-cells, and individual bacteria. *GranSim* simulates a two-dimensional section of lung tissue (6mm x 6mm) represented by dissecting a 300 x 300 grid into 90,000 grid microcompartments, each of size 20μm. Simulations begin with a single infected macrophage in the center of the grid that initiates recruitment of additional macrophages and T cells to the infection site. These immune cells interact with each other and with Mtb according to a large set of immunology-based rules that describe killing of Mtb, secretion of chemokines/cytokines, and activation and movement of cells (for a complete description of our rules, see http://malthus.micro.med.umich.edu/GranSim/). Granulomas "emerge" as a result of these interactions when simulating *GranSim.* Infection is initiated with a single bacterium.

NHPs are highly informative animal models for TB, as TB disease and pathology, including granulomas, are similar to humans [69]. The immunological rules and cellular behaviors included in *GranSim* are based on datasets derived from NHP granulomas [65, 66, 68]. Moreover, we validate and calibrate *GranSim* granulomas to both spatial and temporal datasets from NHP granulomas, including immune cells (macrophages and T

cells) and Mtb counts and the spatial distribution of cell types within a granuloma [30, 50, 70]. *GranSim* simulates a broad range of biologically relevant outcomes that can recreate the heterogeneity of observed granulomas from NHPs and humans [66, 71] .

Antibiotics may have bactericidal (bacterial killing) or bacteriostatic (inhibition of bacterial growth) effects. To capture the actions of these drugs on bacteria, tracking the individual bacteria within the granuloma is key [72]. To mimic that of actual infection, we simulate three distinct subpopulations of Mtb based on their location within granulomas: replicating-extracellular Mtb, intracellular Mtb that reside and replicate within macrophages, and Mtb that are trapped within the caseous necrotic core. These caseum-trapped bacteria have varying growth rates depending on the level of tissue caseation. These subpopulations differ in their abilities to replicate and move within a granuloma.

Latin Hypercube Sampling (LHS)

LHS is a parameter-sampling method that samples the parameter space without replacement and covers the parameter space more uniformly than a simple random sampling. It is done by dividing each parameter distribution into N equal probability intervals and sampling from these intervals to generate *N* distinct parameter sets and identify epistemic uncertainty [48, 73, 74]. We used this method to generate an *in silico* library of granulomas in *GranSim*. If the system under study, as is ours, has stochastic components, it is necessary to do replicates (we choose 3) of each of the *N* runs to capture the aleatory uncertainty within as well (c.f. [48]). These samplings capture both epistemic and aleatory uncertainty that arise in parameter sets.

546 **Pharmacokinetic/pharmacodynamic (PK/PD) modeling**

547 We have used *GranSim* previously to simulate the PK/PD of antibiotic drug treatment for
548 TB. Specifically, we can simulate the spatial distribution of antibiotics and their sterilizing
549 ability for different antibiotic regimens [5, 6, 8, 38].

550 Briefly, the PK/PD model within *GranSim* simulates the plasma concentration over
551 time following oral doses of antibiotics, the subsequent spatial concentration in the
552 simulated granuloma and the bactericidal activity based on the local concentration. We
553 modeled the plasma PK using a compartmental, ordinary differential equation model to
554 simulate absorption through transit compartments into the plasma, exchange with
555 peripheral tissue and first-order elimination from the plasma [6, 22]. To simulate tissue
556 PK, we referenced the concentration in the plasma and calculated flux through vascular
557 sources on the computational grid, diffusion through tissue, binding to caseum and
558 epithelium and partitioning into macrophages [6, 8, 38, 75].

559 We modeled the PD by using a Hill function that determines the concentration (*C*)
560 dependent antibiotic killing rate constant (*k*), which is the rate of bacterial death per time
561 step [76]. The general form of the Hill curve we use is:

562 $$k(C) = E_{max}\frac{C^h}{C^h + {C_{50}}^h} \quad \text{(Eq.1)}$$

563 where E_{max} is the maximum killing rate constant, h is the Hill coefficient and C_{50} is the
564 concentration needed to achieve the half maximal killing rate constant ($E_{max}/2$). For each
565 antibiotic, we calibrated the parameters of the Hill curve (E_{max}, C_{50} and h) for intracellular,
566 replicating-extracellular and caseum Mtb separately, as the pharmacodynamics of
567 antibiotics are different in these subpopulations. The calibration is based on bactericidal
568 assays of infected macrophages [18, 19, 77-79], Mtb in rich growth media [18, 19, 77-79]

569 and Mtb in caseum mimic [20], for intracellular, replicating-extracellular and Mtb in
570 caseum, respectively.

571 In this study, we used the effective concentration of each antibiotic (*C*) as the total
572 concentration in each grid compartment rather than the free concentration, i.e., the
573 extracellular concentration that is not bound to any macromolecules or any tissue, as we
574 calculated in our previous studies [8, 57]. We made this change as the bactericidal assays
575 we reference are based on the total concentration applied to the Mtb *in vitro* [20].

576

577 **Accounting for pharmacodynamic drug interactions in the model**

578 When multiple antibiotics are used and thus present and available on our simulation grid
579 within *GranSim*, we simulate their interaction by adjusting the effective concentration
580 according to their predicted fractional inhibitory concentration (FIC) values, as we have
581 done previously [57]. We use the FIC values predicted by an *in silico* tool, INDIGO-MTB
582 (inferring drug interactions using chemogenomics and orthology optimized for Mtb) [31,
583 32]. This tool employs a machine learning algorithm that uses known drug interactions
584 along with drug transcriptomics data as inputs and predicts unknown drug interactions,
585 i.e., FICs.

586 Briefly, we first converted the concentrations of all antibiotics on a small section of
587 the grid (microgrid) to the equipotent concentration of the antibiotic of the highest maximal
588 killing rate constant (highest E_{max}). For example, if we have two antibiotics (drug 1 with
589 the concentration C_1 and drug 2 with the concentration C_2) and drug 1 has a higher E_{max},
590 then we calculate the adjusted concentration for drug 2 ($C_{2,adj}$), which is the concentration

of drug 1 that results in the same antibiotic killing rate constant as drug 2 with the concentration of C_2, with the following equation:

$$C_1 = C_{2,adj} = \left(\frac{{C_{1,50}}^{h_1} {C_2}^{h_2}}{\frac{E_{max,1}}{E_{max,2}} \left({C_2}^{h_2} + {C_{2,50}}^{h_2} \right) - {C_2}^{h_2}} \right)^{1/h_1} \quad \text{(Eq.2)}$$

where $C_{1,50}$ and $C_{2,50}$ are the concentration of C_1 and C_2 at which half maximal killing is achieved, respectively, $E_{max,1}$ and $E_{max,2}$ are the maximal killing rate constants of drug 1 and drug 2, respectively, and h_1 and h_2 are the Hill coefficients of drug 1 and drug 2, respectively. Then, we calculated the effective concentration (C_{eff}) as the sum of the adjusted concentrations of n antibiotics that are increased/decreased based on the FIC values (see S1 Table for a complete list of FIC values) to simulate synergistic/antagonistic effects with the following equation:

$$C_{eff} = \left(\sum_{i=1}^{n} {C_{i,adj}}^{FIC} \right)^{1/FIC} \quad \text{(Eq.3)}$$

where $C_{i,adj}$ is the adjusted concentration of the drug i. Then, we used C_{eff} to calculate the antibiotic killing rate constant k on that microgrid by using the Hill equation constants of the antibiotic with the highest E_{max}:

$$k(C_{eff}) = E_{max} \frac{{C_{eff}}^{h}}{{C_{eff}}^{h} + {C_{50}}^{h}} \quad \text{(Eq.4)}$$

where E_{max}, h and C_{50} are the Hill equation parameters of the antibiotic with the highest E_{max} within the regimen.

Simulating antibiotic regimens in *GranSim*

We calibrated plasma and tissue PK parameters for isoniazid, rifampicin, pyrazinamide and moxifloxacin based on human data [21] and the parameters for ethambutol from

612 rabbit samples [60] as human data are not available for this antibiotic. We also utilized
613 MALDI-MS images from human [21] and rabbit [58, 60] samples that show the spatial
614 distribution of antibiotics within granulomas as a validation for our tissue PK calibration.

615 We simulated regimens on 200 randomly selected granulomas from our *in silico*
616 granuloma library (100 low CFU and 100 high CFU granulomas). We employed different
617 dosing protocols based on the studies shown in Table 1. First, we simulated the protocols
618 for the REMoxTB clinical trial [33] using *GranSim*. There were 3 different groups in this
619 study: control group (HRZE), HRZM group and RMZE group. To simulate the control
620 group, we dosed granulomas with HRZE daily for 8 weeks, followed by 18 weeks of daily
621 dosing of HR. We simulated HRZM and RMZE groups by dosing granulomas for 17 weeks
622 daily with HRZM and RMZE, respectively, followed by 9 weeks of a placebo phase, i.e.,
623 9 weeks of no antibiotics (Table 1).

624 To compare our results to NHP studies performed herein, we simulated the
625 regimens HRZE, HMZE and RMZE for 60 days by dosing daily. We also simulated a
626 positive control case with the same granulomas but with no antibiotics (Table 1).
627 Additionally, we simulated all 2-way, 3-way and 4-way combinations of HRZEM until all
628 granulomas sterilize or reach a stable state, i.e., until the fraction of granulomas that are
629 not sterilized doesn't change significantly over time (120 days for 4-way combinations (5
630 regimens), 220 days for 3-way combinations (10 regimens), 300 days for 2-way
631 combinations (10 regimens)) (Table 1).

632

633 **Average sterilization time measurement**

A regimen's efficacy depends on how fast it can clear all Mtb within a granuloma. Therefore, we measured the average time a regimen needs to clear a granuloma, i.e., *average sterilization time*, as a way to assess regimens' potency. The average sterilization time of a regimen *i* (t_{ster_i}) is

$$t_{ster_i} = \frac{\sum_{k=1}^{n} t_{ster_{i_k}}}{n} \quad \text{(Eq.5)}$$

where *n* is the number of granulomas treated by *i* and $t_{ster_{i_k}}$ is the time that granuloma *k* is treated with *i* until total Mtb within *k* is zero. If a granuloma *k* is not sterilized by a regimen *i* at the end of the treatment, then we assign $t_{ster_{i_k}} = t_{treatment}$ where $t_{treatment}$ is the duration of the treatment.

NHP granuloma FDG avidity measurement in *GranSim*

Positron Emission Tomography and Computed Tomography (PET-CT) scans are used to measure metabolic activity of granulomas within NHP by quantifying the uptake of a glucose analog FDG (2-deoxy-2-[18F]-fluoro-D-glucose) via a measure called SUVR (standardized uptake value ratio) [51]. As a proxy for capturing the SUVR per granuloma from NHP experiments within our computational model, we developed a surrogate measurement in *GranSim* that combines the amount of proinflammatory activity derived from both tumor necrosis factor (TNF) with activity of proinflammatory cells (such as activated T cells and macrophages) that we define as FDG avidity. This is a way to represent the metabolic activity in the *in silico* granulomas. Specifically, we calculate FDG avidity measure for each granuloma, *i* as:

$$FDG\ avidity_i = \sum_{k=1}^{n} \left(TNF_k + M_{r_k} + 4M_{i_k} + 9M_{ci_k} + 6M_{a_k} + 3T_{gam_k} + 3T_{cyt_k}\right) \quad \text{(Eq.6)}$$

where *n* is the number of grid microcompartments of the agent-based model grid in a simulation, TNF_k is the TNF concentration within the microgrid *k* in pg/ml (with an upper bound as 30 pg/ml), M_{r_k}, M_{i_k}, M_{ci_k}, M_{a_k}, $T_{gam_k}$and T_{cyt_k} are the number of resting macrophages, infected macrophages, chronically infected macrophages, active macrophages, IFN-γ producing T cells and cytotoxic T cells at microgrid k, respectively (see S1 Fig for the visualization of FDG avidity in *GranSim* and see http://malthus.micro.med.umich.edu/GranSim/ for more information about the roles of each cell type). The weights that each cell type contributes to the FDG avidity on a grid is determined based on the assumed inflammatory responses each cell type creates based on their *in vivo* activity. Because we do not know all factors or cells that contribute to the SUVR, we use levels of TNF (an inflammatory marker) as a surrogate to represent contributions from other cells to the metabolic activity within a granuloma

Objective functions for regimen optimization

We use two objective functions to be minimized, the average sterilization time (described above) and the total normalized dose (*d*). We define the total normalized dose *d* as

$$d(x) = \sum_{k=1}^{n} \frac{D_i}{D_{i_{max}}}, \quad \text{(Eq.7)}$$

where *k* is the number of antibiotics in the regimen *x*, D_i stands for the dose of the individual antibiotic *i*, and $D_{i_{max}}$ is the maximum allowed dose in our simulations. Minimizing drug dose will decrease potential side effects. In our optimization pipeline, we aim to find the regimens that minimize both objective functions.

The sampling ranges for each dose variable were set to range from 0 mg/kg to double the standard CDC dose [4]. Maximum safe doses for each antibiotic were set to

679 10, 20, 40, 50 and 14 mg/kg for H, R, E, Z and M, respectively, as higher doses would
680 increase the risk of toxicity and would not be clinically relevant [54, 80-83].
681
682 **Kriging-based surrogate model**
683 The goal of a multi-objective optimization is to find the optimal trade-off between two or
684 more objectives by identifying the optimal variable combinations [84]. For example, in this
685 study the goal is to both minimize time to sterilization and drug doses between multiple
686 drugs. Using a surrogate-assisted framework involves predicting the objective functions
687 based on the outcomes of the already-sampled regimens. These predictions can then be
688 used as a computationally inexpensive alternative to predict the objective functions
689 throughout the whole design space.
690 Here, we use a kriging-based surrogate model to generate the objective function
691 predictions. This kriging-based prediction and optimization algorithm is based on a set of
692 open-source MATLAB functions developed by Forrester and Sóbester [62, 85]. This
693 surrogate-assisted framework provides an efficient and accurate way to thoroughly
694 investigate the regimen design space and predict optimal doses but with few iterations as
695 compared to, for example, a genetic algorithm [37]. Based on the sampled regimens and
696 the calculated values of the corresponding objective functions, the algorithm builds a
697 kriging-based, surrogate model to predict the values of the objective functions at any point
698 in the variable design space.
699 The kriging model operates by assuming that the value of a function f of n variables
700 at any n-dimensional vector x can be stated as the sum of some unknown mean (μ) and
701 an error term that is a function of position $\epsilon(x)$ [86]:

$$f(x) = \mu + \in (x) \quad \text{(Eq.8)}$$

We also assume that the error term $\epsilon(x)$ is normally distributed with a mean of 0 and a standard deviation of σ^2. To provide an estimate for the error at any given *x*, we assume the errors at two points are correlated based on the distance between those two points. This means points that are closer in the variable space tend to be more related and have smaller variance than those that are farther. Hence, the correlation in error between points *i* and *j*, equal to component R_{ij} in the correlation matrix *R*, exponentially decays with respect to the weighted distance between them:

$$R_{ij} = Corr\left[\in (x^{(i)}), \in (x^{(j)})\right] = exp\left[-\sum_{h=1}^{n} \theta_h \left| x_h^{(i)} - x_h^{(j)} \right|^{p_h} \right] (\theta_h \geq 0, p_h \in [1,2]) \quad \text{(Eq.9)}$$

where θ_h and p_h are correlation parameters. Here, the correlation varies between 0 and 1 for the farthest and closest points, respectively. The aim in this optimization algorithm is to estimate the parameters μ, σ^2, θ_h and p_h for h=1,..,n that maximizes the likelihood function *L*:

$$L = \frac{1}{(2\pi\hat{\sigma}^2)^{k/2} |\boldsymbol{R}|^{1/2}} exp\left[-\frac{(\boldsymbol{y} - \boldsymbol{1}\hat{\mu})' \boldsymbol{R}^{-1} (\boldsymbol{y} - \boldsymbol{1}\hat{\mu})}{2\hat{\sigma}^2} \right] \quad \text{(Eq.10)}$$

where *y* is a vector of length *k* with the values of the observed data at each of the sample points. By varying θ_h and p_h to find their optimal values that maximizes the likelihood function *L*, we can calculate μ and σ^2 and, hence, can predict the value of *f* at any point *x*.

Pareto optimization

For multi-objective optimization goals, there may be a trade-off between different objectives. For example, increasing the dose of each antibiotic in a regimen to the maximal dose would result in a minimal sterilization time at the cost of a very high dose,

which may lead to severe side effects. Similarly, a very low dose would minimize the total dose of a regimen; however, the granuloma would sterilize slowly, if at all. Both solutions are a part of a Pareto set, which contains (non-dominated) optimal solutions using *different* weights on the objectives. Therefore, we need to derive compromised solutions, deciding weights between the objectives within the algorithm (see S1 Appendix and S2 Fig for a detailed description of a Pareto set). By using the predicted objective functions, our algorithm selects a new regimen that maximizes the likelihood of expected improvement of the Pareto set. Specifically, the expected improvement criterion seeks the regimen(s) that maximize(s) the expected distance from the points currently in the Pareto front and lies in the blue shaded area in S2 Fig, where new solutions would dominate the current Pareto set [62, 87].

Optimization pipeline in *GranSim*

Our optimization pipeline started with exploring an initial set of 40 regimens for each set of 4-way combinations (HRZE, HRZM, RMZE, HMZE, HRME). We generated these 40 regimens using the LHS sampling scheme for the parameter space of doses for each individual antibiotic. These were varied between 0 to the double of the standard CDC dose [4], i.e., 10, 20, 50, 40 and 14 for H, R, Z, E and M, respectively. For each regimen, we simulated 30 granulomas (15 high-CFU and 15 low-CFU granulomas) each for 180 days (Table 1) and averaged their sterilization times to evaluate the objective function for each regimen. Then, by using the multi-objective surrogate-assisted optimization algorithm, we predicted the objective functions and one regimen that is expected to improve the current Pareto set. We simulated this new regimen using *GranSim* on the 30

748 total high- and low-CFU granulomas. This iterative process continued for 20 iterations,
749 and one optimal regimen was simulated at the end of each iteration. At the end of this
750 pipeline, we computed the Pareto front, i.e., the optimal non-dominating regimens.
751
752 **Nonhuman primate model for *in vivo* regimen experimental studies**
753 Nine male Chinese cynomolgus macaques (*Macaca fascicularis*) (4-7 years of age) were
754 dedicated to this study and were infected with virulent *M. tuberculosis* strain Erdman (8-
755 21 CFU) via bronchoscopic instillation into a lower lobe. Three months post-infection, drug
756 treatment was initiated and continued for 2 months, then the animals were necropsied.
757 Animals were monitored daily for appetite and behavior and monthly for weight and
758 erythrocyte sedimentation rate (a sign of inflammation). Gastric aspirate and BAL
759 samples were cultured for Mtb to assess disease progression. An additional seven
760 cynomolgus macaques (2 males, 3 females, 5-9 years of age, infected with Mtb Erdman)
761 from a concurrent study were included here as historical untreated controls and
762 necropsied 5 months post-infection.
763 Drug treatments were 1. isoniazid (H), rifampicin (R), pyrazinamide (Z) and
764 ethambutol (E) (HRZE, N=3); 2. isoniazid (H), moxifloxacin (M), pyrazinamide (Z) and
765 ethambutol (E) (HMZE, N=4); or 3. rifampicin (R), moxifloxacin (M), pyrazinamide (Z) and
766 ethambutol (E) (RMZE, N=2). Drug dosing as follows: H: 15 mg/kg; R: 20 mg/kg; Z: 150
767 mg/kg; E 55 mg/kg; M: 35 mg/kg. Drugs were provided daily in treats or by gavage.
768 Macaques were treated for 2 months, and drugs were stopped one day before
769 necropsy. See Table 1 for a list of treatment protocols.

^{18}F-fluorodeoxyglucose (FDG) PET-CT imaging was performed prior to treatment initiation and at 4- and 8-weeks post-treatment initiation. FDG is a glucose analogue, which is preferentially taken up by and retained in metabolically active cells and thus is useful as a proxy for inflammation. FDG uptake was quantified using the peak standard uptake value (SUV) associated with each granuloma, as previously described [51].

Detailed necropsies were performed using the final PET-CT scan as a map to isolate all lesions (granulomas, consolidations, etc.), uninvolved lung lobe samples, all thoracic lymph nodes, peripheral lymph nodes, spleen and liver. All samples were plated individually for Mtb on 7H11 plates, incubated for 3 weeks in a 5% C02 incubator. Bacterial burden for each sample was calculated based on colonies counted on plates. Sum of all samples in thoracic cavity (lung, granulomas, lymph nodes) is reported as total thoracic CFU; total lung and total thoracic LN are also calculated.

Acknowledgment

We thank Dr. Simeone Marino for his contributions by developing the rules for FDG avidity measurement in *GranSim*. We thank Paul Wolberg for computational assistance and support. We are grateful to the veterinary and research technical staff in the Flynn lab for their work on this study. This research was supported by NIH Grants R01 AI50684 (DEK, JLF), U01 HL131072 (DEK, VAD, JJL, JLF), S10 OD023524 (VAD) and supported in part by funding by the Wellcome Leap ΔTissue Program awarded to (DEK, JJL, JLF). Further funding comes from a contract grant from the MRI Bill & Melinda Gates Foundation awarded to DEK. Simulations also use resources of the National Energy Research Scientific Computing Center, which is supported by the Office of Science of the U.S.

Department of Energy under Contract No. ACI-1053575 and the Extreme Science and Engineering Discovery Environment (XSEDE), which is supported by National Science Foundation Grant MCB140228.

References

1. Global tuberculosis report 2022. Geneva: World Health Organization; 2022.
2. Bahuguna A, Rawat DS. An overview of new antitubercular drugs, drug candidates, and their targets. Med Res Rev. 2020;40(1):263-92. Epub 20190628. doi: 10.1002/med.21602. PubMed PMID: 31254295.
3. Peloquin CA, Davies GR. The Treatment of Tuberculosis. Clin Pharmacol Ther. 2021;110(6):1455-66. Epub 20210605. doi: 10.1002/cpt.2261. PubMed PMID: 33837535.
4. Nahid P, Dorman SE, Alipanah N, Barry PM, Brozek JL, Cattamanchi A, et al. Executive Summary: Official American Thoracic Society/Centers for Disease Control and Prevention/Infectious Diseases Society of America Clinical Practice Guidelines: Treatment of Drug-Susceptible Tuberculosis. Clin Infect Dis. 2016;63(7):853-67. doi: 10.1093/cid/ciw566. PubMed PMID: 27621353; PubMed Central PMCID: PMCPMC6366011.
5. Pienaar E, Sarathy J, Prideaux B, Dietzold J, Dartois V, Kirschner DE, et al. Comparing efficacies of moxifloxacin, levofloxacin and gatifloxacin in tuberculosis granulomas using a multi-scale systems pharmacology approach. PLoS Comput Biol. 2017;13(8):e1005650. Epub 20170817. doi: 10.1371/journal.pcbi.1005650. PubMed PMID: 28817561; PubMed Central PMCID: PMCPMC5560534.
6. Pienaar E, Cilfone NA, Lin PL, Dartois V, Mattila JT, Butler JR, et al. A computational tool integrating host immunity with antibiotic dynamics to study tuberculosis treatment. J Theor Biol. 2015;367:166-79. Epub 20141209. doi: 10.1016/j.jtbi.2014.11.021. PubMed PMID: 25497475; PubMed Central PMCID: PMCPMC4332617.
7. Sarathy JP, Zuccotto F, Hsinpin H, Sandberg L, Via LE, Marriner GA, et al. Prediction of Drug Penetration in Tuberculosis Lesions. ACS Infect Dis. 2016;2(8):552-63. Epub 20160706. doi: 10.1021/acsinfecdis.6b00051. PubMed PMID: 27626295; PubMed Central PMCID: PMCPMC5028112.
8. Cicchese JM, Dartois V, Kirschner DE, Linderman JJ. Both Pharmacokinetic Variability and Granuloma Heterogeneity Impact the Ability of the First-Line Antibiotics to Sterilize Tuberculosis Granulomas. Front Pharmacol. 2020;11:333. Epub 2020/03/24. doi: 10.3389/fphar.2020.00333. PubMed PMID: 32265707; PubMed Central PMCID: PMCPMC7105635.
9. Sacchettini JC, Rubin EJ, Freundlich JS. Drugs versus bugs: in pursuit of the persistent predator Mycobacterium tuberculosis. Nat Rev Microbiol. 2008;6(1):41-52. doi: 10.1038/nrmicro1816. PubMed PMID: 18079742.
10. Walter ND, Dolganov GM, Garcia BJ, Worodria W, Andama A, Musisi E, et al. Transcriptional Adaptation of Drug-tolerant Mycobacterium tuberculosis During Treatment of

Human Tuberculosis. J Infect Dis. 2015;212(6):990-8. Epub 20150311. doi: 10.1093/infdis/jiv149. PubMed PMID: 25762787; PubMed Central PMCID: PMCPMC4548467.

11. Gold B, Nathan C. Targeting Phenotypically Tolerant Mycobacterium tuberculosis. Microbiol Spectr. 2017;5(1). doi: 10.1128/microbiolspec.TBTB2-0031-2016. PubMed PMID: 28233509; PubMed Central PMCID: PMCPMC5367488.

12. Pasipanodya JG, McIlleron H, Burger A, Wash PA, Smith P, Gumbo T. Serum drug concentrations predictive of pulmonary tuberculosis outcomes. J Infect Dis. 2013;208(9):1464-73. Epub 20130729. doi: 10.1093/infdis/jit352. PubMed PMID: 23901086; PubMed Central PMCID: PMCPMC3789573.

13. Ormerod LP. Multidrug-resistant tuberculosis (MDR-TB): epidemiology, prevention and treatment. Br Med Bull. 2005;73-74:17-24. Epub 20050614. doi: 10.1093/bmb/ldh047. PubMed PMID: 15956357.

14. Dartois VA, Rubin EJ. Anti-tuberculosis treatment strategies and drug development: challenges and priorities. Nat Rev Microbiol. 2022;20(11):685-701. Epub 20220427. doi: 10.1038/s41579-022-00731-y. PubMed PMID: 35478222; PubMed Central PMCID: PMCPMC9045034.

15. Pasipanodya JG, Nuermberger E, Romero K, Hanna D, Gumbo T. Systematic Analysis of Hollow Fiber Model of Tuberculosis Experiments. Clin Infect Dis. 2015;61 Suppl 1:S10-7. doi: 10.1093/cid/civ425. PubMed PMID: 26224767.

16. Srivastava S, Boorgula GD, Wang JY, Huang HL, Howe D, Gumbo T, et al. Rifampin Pharmacokinetics/Pharmacodynamics in the Hollow-Fiber Model of Mycobacterium kansasii Infection. Antimicrob Agents Chemother. 2022;66(4):e0232021. Epub 20220322. doi: 10.1128/aac.02320-21. PubMed PMID: 35315686; PubMed Central PMCID: PMCPMC9017304.

17. Gumbo T, Louie A, Liu W, Ambrose PG, Bhavnani SM, Brown D, et al. Isoniazid's bactericidal activity ceases because of the emergence of resistance, not depletion of Mycobacterium tuberculosis in the log phase of growth. J Infect Dis. 2007;195(2):194-201. Epub 20061207. doi: 10.1086/510247. PubMed PMID: 17191164.

18. Jayaram R, Shandil RK, Gaonkar S, Kaur P, Suresh BL, Mahesh BN, et al. Isoniazid pharmacokinetics-pharmacodynamics in an aerosol infection model of tuberculosis. Antimicrob Agents Chemother. 2004;48(8):2951-7. doi: 10.1128/AAC.48.8.2951-2957.2004. PubMed PMID: 15273105; PubMed Central PMCID: PMCPMC478500.

19. Jayaram R, Gaonkar S, Kaur P, Suresh BL, Mahesh BN, Jayashree R, et al. Pharmacokinetics-pharmacodynamics of rifampin in an aerosol infection model of tuberculosis. Antimicrob Agents Chemother. 2003;47(7):2118-24. doi: 10.1128/AAC.47.7.2118-2124.2003. PubMed PMID: 12821456; PubMed Central PMCID: PMCPMC161844.

20. Sarathy JP, Via LE, Weiner D, Blanc L, Boshoff H, Eugenin EA, et al. Extreme Drug Tolerance of Mycobacterium tuberculosis in Caseum. Antimicrob Agents Chemother. 2018;62(2). Epub 20180125. doi: 10.1128/AAC.02266-17. PubMed PMID: 29203492; PubMed Central PMCID: PMCPMC5786764.

21. Prideaux B, Via LE, Zimmerman MD, Eum S, Sarathy J, O'Brien P, et al. The association between sterilizing activity and drug distribution into tuberculosis lesions. Nat Med. 2015;21(10):1223-7. Epub 20150907. doi: 10.1038/nm.3937. PubMed PMID: 26343800; PubMed Central PMCID: PMCPMC4598290.

22. Kjellsson MC, Via LE, Goh A, Weiner D, Low KM, Kern S, et al. Pharmacokinetic evaluation of the penetration of antituberculosis agents in rabbit pulmonary lesions. Antimicrob Agents Chemother. 2012;56(1):446-57. Epub 20111010. doi: 10.1128/AAC.05208-11. PubMed PMID: 21986820; PubMed Central PMCID: PMCPMC3256032.
23. Dartois V. The path of anti-tuberculosis drugs: from blood to lesions to mycobacterial cells. Nat Rev Microbiol. 2014;12(3):159-67. Epub 2014/02/03. doi: 10.1038/nrmicro3200. PubMed PMID: 24487820; PubMed Central PMCID: PMCPMC4341982.
24. Cokol M, Kuru N, Bicak E, Larkins-Ford J, Aldridge BB. Efficient measurement and factorization of high-order drug interactions in. Sci Adv. 2017;3(10):e1701881. Epub 2017/10/11. doi: 10.1126/sciadv.1701881. PubMed PMID: 29026882; PubMed Central PMCID: PMCPMC5636204.
25. Larkins-Ford J, Greenstein T, Van N, Degefu YN, Olson MC, Sokolov A, et al. Systematic measurement of combination drug landscapes to predict i*n vivo* treatment outcomes for tuberculosis. bioRxiv. 2021. doi: 10.1101/2021.02.03.429579.
26. Drusano GL, Neely M, Van Guilder M, Schumitzky A, Brown D, Fikes S, et al. Analysis of combination drug therapy to develop regimens with shortened duration of treatment for tuberculosis. PLoS One. 2014;9(7):e101311. Epub 20140708. doi: 10.1371/journal.pone.0101311. PubMed PMID: 25003557; PubMed Central PMCID: PMCPMC4086932.
27. Grosset JH, Tyagi S, Almeida DV, Converse PJ, Li SY, Ammerman NC, et al. Assessment of clofazimine activity in a second-line regimen for tuberculosis in mice. Am J Respir Crit Care Med. 2013;188(5):608-12. doi: 10.1164/rccm.201304-0753OC. PubMed PMID: 23822735; PubMed Central PMCID: PMCPMC3827279.
28. Tasneen R, Betoudji F, Tyagi S, Li SY, Williams K, Converse PJ, et al. Contribution of Oxazolidinones to the Efficacy of Novel Regimens Containing Bedaquiline and Pretomanid in a Mouse Model of Tuberculosis. Antimicrob Agents Chemother. 2016;60(1):270-7. Epub 20151026. doi: 10.1128/AAC.01691-15. PubMed PMID: 26503656; PubMed Central PMCID: PMCPMC4704221.
29. Via LE, England K, Weiner DM, Schimel D, Zimmerman MD, Dayao E, et al. A sterilizing tuberculosis treatment regimen is associated with faster clearance of bacteria in cavitary lesions in marmosets. Antimicrob Agents Chemother. 2015;59(7):4181-9. Epub 20150504. doi: 10.1128/AAC.00115-15. PubMed PMID: 25941223; PubMed Central PMCID: PMCPMC4468655.
30. Lin PL, Coleman T, Carney JP, Lopresti BJ, Tomko J, Fillmore D, et al. Radiologic Responses in Cynomolgus Macaques for Assessing Tuberculosis Chemotherapy Regimens. Antimicrob Agents Chemother. 2013;57(9):4237-44. Epub 20130624. doi: 10.1128/AAC.00277-13. PubMed PMID: 23796926; PubMed Central PMCID: PMCPMC3754323.
31. Chandrasekaran S, Cokol-Cakmak M, Sahin N, Yilancioglu K, Kazan H, Collins JJ, et al. Chemogenomics and orthology-based design of antibiotic combination therapies. Mol Syst Biol. 2016;12(5):872. Epub 20160524. doi: 10.15252/msb.20156777. PubMed PMID: 27222539; PubMed Central PMCID: PMCPMC5289223.
32. Ma S, Jaipalli S, Larkins-Ford J, Lohmiller J, Aldridge BB, Sherman DR, et al. Transcriptomic Signatures Predict Regulators of Drug Synergy and Clinical Regimen Efficacy against Tuberculosis. mBio. 2019;10(6). Epub 20191112. doi: 10.1128/mBio.02627-19. PubMed PMID: 31719182; PubMed Central PMCID: PMCPMC6851285.

33. Gillespie SH, Crook AM, McHugh TD, Mendel CM, Meredith SK, Murray SR, et al. Four-month moxifloxacin-based regimens for drug-sensitive tuberculosis. N Engl J Med. 2014;371(17):1577-87. Epub 20140907. doi: 10.1056/NEJMoa1407426. PubMed PMID: 25196020; PubMed Central PMCID: PMCPMC4277680.
34. Merle CS, Fielding K, Sow OB, Gninafon M, Lo MB, Mthiyane T, et al. A four-month gatifloxacin-containing regimen for treating tuberculosis. N Engl J Med. 2014;371(17):1588-98. doi: 10.1056/NEJMoa1315817. PubMed PMID: 25337748.
35. Jindani A, Harrison TS, Nunn AJ, Phillips PP, Churchyard GJ, Charalambous S, et al. High-dose rifapentine with moxifloxacin for pulmonary tuberculosis. N Engl J Med. 2014;371(17):1599-608. doi: 10.1056/NEJMoa1314210. PubMed PMID: 25337749; PubMed Central PMCID: PMCPMC4233406.
36. Controlled clinical trial of four short-course (6-month) regimens of chemotherapy for treatment of pulmonary tuberculosis. Lancet. 1974;2(7889):1100-6. PubMed PMID: 4139405.
37. Cicchese JM, Pienaar E, Kirschner DE, Linderman JJ. Applying optimization algorithms to tuberculosis antibiotic treatment regimens. Cell Mol Bioeng. 2017;10(6):523-35. Epub 2017/08/30. doi: 10.1007/s12195-017-0507-6. PubMed PMID: 29276546; PubMed Central PMCID: PMCPMC5737793.
38. Pienaar E, Dartois V, Linderman JJ, Kirschner DE. In silico evaluation and exploration of antibiotic tuberculosis treatment regimens. BMC Syst Biol. 2015;9:79. Epub 20151114. doi: 10.1186/s12918-015-0221-8. PubMed PMID: 26578235; PubMed Central PMCID: PMCPMC4650854.
39. Nuermberger EL, Yoshimatsu T, Tyagi S, Williams K, Rosenthal I, O'Brien RJ, et al. Moxifloxacin-containing regimens of reduced duration produce a stable cure in murine tuberculosis. Am J Respir Crit Care Med. 2004;170(10):1131-4. Epub 20040811. doi: 10.1164/rccm.200407-885OC. PubMed PMID: 15306535.
40. Nuermberger EL, Yoshimatsu T, Tyagi S, O'Brien RJ, Vernon AN, Chaisson RE, et al. Moxifloxacin-containing regimen greatly reduces time to culture conversion in murine tuberculosis. Am J Respir Crit Care Med. 2004;169(3):421-6. Epub 20031024. doi: 10.1164/rccm.200310-1380OC. PubMed PMID: 14578218.
41. Dorman SE, Johnson JL, Goldberg S, Muzanye G, Padayatchi N, Bozeman L, et al. Substitution of moxifloxacin for isoniazid during intensive phase treatment of pulmonary tuberculosis. Am J Respir Crit Care Med. 2009;180(3):273-80. Epub 20090430. doi: 10.1164/rccm.200901-0078OC. PubMed PMID: 19406981.
42. Rustomjee R, Lienhardt C, Kanyok T, Davies GR, Levin J, Mthiyane T, et al. A Phase II study of the sterilising activities of ofloxacin, gatifloxacin and moxifloxacin in pulmonary tuberculosis. Int J Tuberc Lung Dis. 2008;12(2):128-38. PubMed PMID: 18230244.
43. Conde MB, Efron A, Loredo C, De Souza GR, Graça NP, Cezar MC, et al. Moxifloxacin versus ethambutol in the initial treatment of tuberculosis: a double-blind, randomised, controlled phase II trial. Lancet. 2009;373(9670):1183-9. doi: 10.1016/S0140-6736(09)60333-0. PubMed PMID: 19345831; PubMed Central PMCID: PMCPMC2866651.
44. De Groote MA, Gilliland JC, Wells CL, Brooks EJ, Woolhiser LK, Gruppo V, et al. Comparative studies evaluating mouse models used for efficacy testing of experimental drugs against Mycobacterium tuberculosis. Antimicrob Agents Chemother. 2011;55(3):1237-47. Epub

960 20101206. doi: 10.1128/AAC.00595-10. PubMed PMID: 21135176; PubMed Central PMCID:
961 PMCPMC3067068.
962 45. Imperial MZ, Nahid P, Phillips PPJ, Davies GR, Fielding K, Hanna D, et al. A patient-level
963 pooled analysis of treatment-shortening regimens for drug-susceptible pulmonary tuberculosis.
964 Nat Med. 2018;24(11):1708-15. Epub 20181105. doi: 10.1038/s41591-018-0224-2. PubMed
965 PMID: 30397355; PubMed Central PMCID: PMCPMC6685538.
966 46. Joslyn LR, Linderman JJ, Kirschner DE. A virtual host model of Mycobacterium tuberculosis
967 infection identifies early immune events as predictive of infection outcomes. J Theor Biol.
968 2022;539:111042. Epub 20220131. doi: 10.1016/j.jtbi.2022.111042. PubMed PMID: 35114195;
969 PubMed Central PMCID: PMCPMC9169921.
970 47. Hult C, Mattila JT, Gideon HP, Linderman JJ, Kirschner DE. Neutrophil Dynamics Affect.
971 Front Immunol. 2021;12:712457. Epub 20211005. doi: 10.3389/fimmu.2021.712457. PubMed
972 PMID: 34675916; PubMed Central PMCID: PMCPMC8525425.
973 48. Marino S, Hogue IB, Ray CJ, Kirschner DE. A methodology for performing global
974 uncertainty and sensitivity analysis in systems biology. J Theor Biol. 2008;254(1):178-96. Epub
975 20080420. doi: 10.1016/j.jtbi.2008.04.011. PubMed PMID: 18572196; PubMed Central PMCID:
976 PMCPMC2570191.
977 49. Lin PL, Flynn JL. The End of the Binary Era: Revisiting the Spectrum of Tuberculosis. J
978 Immunol. 2018;201(9):2541-8. doi: 10.4049/jimmunol.1800993. PubMed PMID: 30348659;
979 PubMed Central PMCID: PMCPMC6217958.
980 50. Gideon HP, Phuah J, Myers AJ, Bryson BD, Rodgers MA, Coleman MT, et al. Variability in
981 tuberculosis granuloma T cell responses exists, but a balance of pro- and anti-inflammatory
982 cytokines is associated with sterilization. PLoS Pathog. 2015;11(1):e1004603. Epub 20150122.
983 doi: 10.1371/journal.ppat.1004603. PubMed PMID: 25611466; PubMed Central PMCID:
984 PMCPMC4303275.
985 51. White AG, Maiello P, Coleman MT, Tomko JA, Frye LJ, Scanga CA, et al. Analysis of 18FDG
986 PET/CT Imaging as a Tool for Studying Mycobacterium tuberculosis Infection and Treatment in
987 Non-human Primates. J Vis Exp. 2017;(127). Epub 20170905. doi: 10.3791/56375. PubMed PMID:
988 28930979; PubMed Central PMCID: PMCPMC5752181.
989 52. Uplekar M, Weil D, Lonnroth K, Jaramillo E, Lienhardt C, Dias HM, et al. WHO's new end
990 TB strategy. Lancet. 2015;385(9979):1799-801. Epub 20150324. doi: 10.1016/S0140-
991 6736(15)60570-0. PubMed PMID: 25814376.
992 53. Park JH, Choe J, Bae M, Choi S, Jung KH, Kim MJ, et al. Clinical Characteristics and
993 Radiologic Features of Immunocompromised Patients With Pauci-Bacillary Pulmonary
994 Tuberculosis Receiving Delayed Diagnosis and Treatment. Open Forum Infect Dis.
995 2019;6(2):ofz002. Epub 20190117. doi: 10.1093/ofid/ofz002. PubMed PMID: 30775402; PubMed
996 Central PMCID: PMCPMC6366656.
997 54. Boeree MJ, Heinrich N, Aarnoutse R, Diacon AH, Dawson R, Rehal S, et al. High-dose
998 rifampicin, moxifloxacin, and SQ109 for treating tuberculosis: a multi-arm, multi-stage
999 randomised controlled trial. Lancet Infect Dis. 2017;17(1):39-49. Epub 20161026. doi:
1000 10.1016/S1473-3099(16)30274-2. PubMed PMID: 28100438; PubMed Central PMCID:
1001 PMCPMC5159618.

55. Boeree MJ, Diacon AH, Dawson R, Narunsky K, du Bois J, Venter A, et al. A dose-ranging trial to optimize the dose of rifampin in the treatment of tuberculosis. Am J Respir Crit Care Med. 2015;191(9):1058-65. doi: 10.1164/rccm.201407-1264OC. PubMed PMID: 25654354.

56. Conradie F, Diacon AH, Ngubane N, Howell P, Everitt D, Crook AM, et al. Treatment of Highly Drug-Resistant Pulmonary Tuberculosis. N Engl J Med. 2020;382(10):893-902. doi: 10.1056/NEJMoa1901814. PubMed PMID: 32130813; PubMed Central PMCID: PMCPMC6955640.

57. Cicchese JM, Sambarey A, Kirschner D, Linderman JJ, Chandrasekaran S. A multi-scale pipeline linking drug transcriptomics with pharmacokinetics predicts in vivo interactions of tuberculosis drugs. Sci Rep. 2021;11(1):5643. Epub 2021/03/11. doi: 10.1038/s41598-021-84827-0. PubMed PMID: 33707554; PubMed Central PMCID: PMCPMC7971003.

58. Blanc L, Daudelin IB, Podell BK, Chen PY, Zimmerman M, Martinot AJ, et al. High-resolution mapping of fluoroquinolones in TB rabbit lesions reveals specific distribution in immune cell types. Elife. 2018;7. Epub 20181114. doi: 10.7554/eLife.41115. PubMed PMID: 30427309; PubMed Central PMCID: PMCPMC6249001.

59. Lakshminarayana SB, Huat TB, Ho PC, Manjunatha UH, Dartois V, Dick T, et al. Comprehensive physicochemical, pharmacokinetic and activity profiling of anti-TB agents. J Antimicrob Chemother. 2015;70(3):857-67. Epub 20141111. doi: 10.1093/jac/dku457. PubMed PMID: 25587994; PubMed Central PMCID: PMCPMC7714050.

60. Zimmerman M, Lestner J, Prideaux B, O'Brien P, Dias-Freedman I, Chen C, et al. Ethambutol Partitioning in Tuberculous Pulmonary Lesions Explains Its Clinical Efficacy. Antimicrob Agents Chemother. 2017;61(9). Epub 20170824. doi: 10.1128/AAC.00924-17. PubMed PMID: 28696241; PubMed Central PMCID: PMCPMC5571334.

61. Tufariello JM, Chan J, Flynn JL. Latent tuberculosis: mechanisms of host and bacillus that contribute to persistent infection. Lancet Infect Dis. 2003;3(9):578-90. doi: 10.1016/s1473-3099(03)00741-2. PubMed PMID: 12954564.

62. Forrester AI, Sóbester A, Keane AJ. Engineering Design via Surrogate Modelling: A Practical Guide. John Wiley & Sons; 2008.

63. Ganchua SKC, White AG, Klein EC, Flynn JL. Lymph nodes-The neglected battlefield in tuberculosis. PLoS Pathog. 2020;16(8):e1008632. Epub 20200813. doi: 10.1371/journal.ppat.1008632. PubMed PMID: 32790739; PubMed Central PMCID: PMCPMC7425845.

64. Wessler T, Joslyn LR, Borish HJ, Gideon HP, Flynn JL, Kirschner DE, et al. A computational model tracks whole-lung Mycobacterium tuberculosis infection and predicts factors that inhibit dissemination. PLoS Comput Biol. 2020;16(5):e1007280. Epub 20200520. doi: 10.1371/journal.pcbi.1007280. PubMed PMID: 32433646; PubMed Central PMCID: PMCPMC7239387.

65. Segovia-Juarez JL, Ganguli S, Kirschner D. Identifying control mechanisms of granuloma formation during M. tuberculosis infection using an agent-based model. J Theor Biol. 2004;231(3):357-76. doi: 10.1016/j.jtbi.2004.06.031. PubMed PMID: 15501468.

66. Ray JC, Flynn JL, Kirschner DE. Synergy between individual TNF-dependent functions determines granuloma performance for controlling Mycobacterium tuberculosis infection. J Immunol. 2009;182(6):3706-17. doi: 10.4049/jimmunol.0802297. PubMed PMID: 19265149; PubMed Central PMCID: PMCPMC3182770.

67. Fallahi-Sichani M, El-Kebir M, Marino S, Kirschner DE, Linderman JJ. Multiscale computational modeling reveals a critical role for TNF-α receptor 1 dynamics in tuberculosis granuloma formation. J Immunol. 2011;186(6):3472-83. Epub 20110214. doi: 10.4049/jimmunol.1003299. PubMed PMID: 21321109; PubMed Central PMCID: PMCPMC3127549.

68. Cilfone NA, Perry CR, Kirschner DE, Linderman JJ. Multi-scale modeling predicts a balance of tumor necrosis factor-α and interleukin-10 controls the granuloma environment during Mycobacterium tuberculosis infection. PLoS One. 2013;8(7):e68680. Epub 20130715. doi: 10.1371/journal.pone.0068680. PubMed PMID: 23869227; PubMed Central PMCID: PMCPMC3711807.

69. Coleman MT, Maiello P, Tomko J, Frye LJ, Fillmore D, Janssen C, et al. Early Changes by (18)Fluorodeoxyglucose positron emission tomography coregistered with computed tomography predict outcome after Mycobacterium tuberculosis infection in cynomolgus macaques. Infect Immun. 2014;82(6):2400-4. Epub 20140324. doi: 10.1128/IAI.01599-13. PubMed PMID: 24664509; PubMed Central PMCID: PMCPMC4019174.

70. Joslyn LR, Kirschner DE, Linderman JJ. : A Calibration Protocol That Utilizes Parameter Density Estimation to Explore Parameter Space and Calibrate Complex Biological Models. Cell Mol Bioeng. 2021;14(1):31-47. Epub 20200915. doi: 10.1007/s12195-020-00650-z. PubMed PMID: 33643465; PubMed Central PMCID: PMCPMC7878626.

71. Fallahi-Sichani M, Marino S, Flynn J, Linderman J, Kirschner D. A systems biology approach for understanding granuloma formation and function in tuberculosis. New York Heidelberg Dordrecht London: Springer; 2013. p. 127-55.

72. Pienaar E, Matern WM, Linderman JJ, Bader JS, Kirschner DE. Multiscale Model of Mycobacterium tuberculosis Infection Maps Metabolite and Gene Perturbations to Granuloma Sterilization Predictions. Infect Immun. 2016;84(5):1650-69. Epub 20160422. doi: 10.1128/IAI.01438-15. PubMed PMID: 26975995; PubMed Central PMCID: PMCPMC4862722.

73. McKay M, Beckman R, Conover W. A comparison of three methods for selecting values of input variables in the analysis of output from a computer code. Technometrics; 1979. p. 239-45.

74. Renardy M, Joslyn LR, Millar JA, Kirschner DE. To Sobol or not to Sobol? The effects of sampling schemes in systems biology applications. Math Biosci. 2021;337:108593. Epub 20210416. doi: 10.1016/j.mbs.2021.108593. PubMed PMID: 33865847; PubMed Central PMCID: PMCPMC8184610.

75. Cilfone NA, Kirschner DE, Linderman JJ. Strategies for efficient numerical implementation of hybrid multi-scale agent-based models to describe biological systems. Cell Mol Bioeng. 2015;8(1):119-36. doi: 10.1007/s12195-014-0363-6. PubMed PMID: 26366228; PubMed Central PMCID: PMCPMC4564133.

76. Ankomah P, Levin BR. Two-drug antimicrobial chemotherapy: a mathematical model and experiments with Mycobacterium marinum. PLoS Pathog. 2012;8(1):e1002487. Epub 20120112. doi: 10.1371/journal.ppat.1002487. PubMed PMID: 22253599; PubMed Central PMCID: PMCPMC3257304.

77. Shandil RK, Jayaram R, Kaur P, Gaonkar S, Suresh BL, Mahesh BN, et al. Moxifloxacin, ofloxacin, sparfloxacin, and ciprofloxacin against Mycobacterium tuberculosis: evaluation of in vitro and pharmacodynamic indices that best predict in vivo efficacy. Antimicrob Agents

Chemother. 2007;51(2):576-82. Epub 20061204. doi: 10.1128/AAC.00414-06. PubMed PMID: 17145798; PubMed Central PMCID: PMCPMC1797767.

78. Zhang Y, Mitchison D. The curious characteristics of pyrazinamide: a review. Int J Tuberc Lung Dis. 2003;7(1):6-21. PubMed PMID: 12701830.

79. Hartkoorn RC, Chandler B, Owen A, Ward SA, Bertel Squire S, Back DJ, et al. Differential drug susceptibility of intracellular and extracellular tuberculosis, and the impact of P-glycoprotein. Tuberculosis (Edinb). 2007;87(3):248-55. Epub 20070126. doi: 10.1016/j.tube.2006.12.001. PubMed PMID: 17258938.

80. Diacon AH, Patientia RF, Venter A, van Helden PD, Smith PJ, McIlleron H, et al. Early bactericidal activity of high-dose rifampin in patients with pulmonary tuberculosis evidenced by positive sputum smears. Antimicrob Agents Chemother. 2007;51(8):2994-6. Epub 20070521. doi: 10.1128/AAC.01474-06. PubMed PMID: 17517849; PubMed Central PMCID: PMCPMC1932511.

81. Xu Y, Wu J, Liao S, Sun Z. Treating tuberculosis with high doses of anti-TB drugs: mechanisms and outcomes. Ann Clin Microbiol Antimicrob. 2017;16(1):67. Epub 20171003. doi: 10.1186/s12941-017-0239-4. PubMed PMID: 28974222; PubMed Central PMCID: PMCPMC5627446.

82. Pasipanodya JG, Gumbo T. Clinical and toxicodynamic evidence that high-dose pyrazinamide is not more hepatotoxic than the low doses currently used. Antimicrob Agents Chemother. 2010;54(7):2847-54. Epub 20100503. doi: 10.1128/AAC.01567-09. PubMed PMID: 20439617; PubMed Central PMCID: PMCPMC2897291.

83. Stass H, Dalhoff A, Kubitza D, Schühly U. Pharmacokinetics, safety, and tolerability of ascending single doses of moxifloxacin, a new 8-methoxy quinolone, administered to healthy subjects. Antimicrob Agents Chemother. 1998;42(8):2060-5. doi: 10.1128/AAC.42.8.2060. PubMed PMID: 9687407; PubMed Central PMCID: PMCPMC105860.

84. Akhtar T, Shoemaker CA. Multi objective optimization of computationally expensive multi-modal functions with RBF surrogates and multi-rule selection. Journal of Global Optimization; 2016. p. 17-32.

85. Sóbester A, Forrester AIJ, Toal DJJ, Tresidder E, Tucker S. Engineering design applications of surrogate-assisted optimization techniques. Optimization and Engineering; 2014. p. 243-65.

86. Jones DR, Schonlau M, Welch WJ. Efficient Global Optimization of Expensive Black-Box Functions. Journal of Global Optimization; 1998. p. 455–92.

87. Keane AJ. Statistical improvement criteria for use in multiobjective design optimization. AIAA Journal; 2006. p. 879-91.